TECHNICAL MEMORANDUM

702

Assessment of the Global Fire Assimilation System (GFASv1)

N. Andela[1], J.W. Kaiser[2,3,4], A. Heil[5], T.T. van Leeuwen[1], M.J. Wooster[4], G.R. van der Werf[1], S. Remy[2], and M.G. Schultz[5]

[1] VU University Amsterdam, Netherlands
[2] ECMWF, United Kingdom
[3] Max-Planck-Institut für Chemie, Germany
[4] Kings College London, United Kingdom
[5] Forschungszentrum Jülich, Germany

June 2013

Produced within the MACC-II project (deliverable D31.2)

European Centre for Medium-Range Weather Forecasts
Europäisches Zentrum für mittelfristige Wettervorhersage
Centre européen pour les prévisions météorologiques à moyen

Series: ECMWF Technical Memoranda

A full list of ECMWF Publications can be found on our web site under:
http://www.ecmwf.int/publications/

Contact: library@ecmwf.int

European Centre for Medium Range Weather Forecasts
Shinfield Park, Reading, Berkshire RG2 9AX, England

Abstract

Fire emissions are a crucial source of atmospheric chemical compounds, and accurate emission estimates are therefore of great importance to predict atmospheric composition and air quality. Within the MACC-II (Monitoring Atmospheric Composition and Climate - Interim Implementation) project, the Global Fire Assimilation System (GFAS) is used to estimate near real-time fire emissions. In this report, we assess the quality of the GFASv1.0 emission estimates, analyse its strengths and weaknesses and make recommendations for future GFAS developments.

The assessment is carried out using several approaches. First an inter-comparison with other global fire emissions inventories and burned area estimates was made. GFASv1.0 emission estimates were compared to two other emission inventories: the Global Fire Emission Database (GFED3.1) and the Fire INventory from the National Center for Atmospheric Research (FINNv1, NCAR). GFASv1.0 (Kaiser et al., 2012) is based on fire radiative power (FRP) retrievals, while FINN (Wiedinmyer et al., 2011) and GFED (van der Werf et al., 2010) use an active fire data product and a burned area retrieval, respectively. All three products rely extensively on data from the Moderate Resolution Imaging Spectroradiometer (MODIS) instruments aboard the Terra and Aqua satellites. Besides the use of different satellite fire data, the three fire emission data products also differ in the details of their algorithms. This primarily concerns the application of different land cover maps, different data on fuel load and fuel consumption, and different methods to account for unobserved scenes. GFAS emission estimates are calculated using biome specific conversion factors to link FRP to GFED dry matter burned. Therefore GFAS emission estimates are dependent on historical GFED data. Therefore also a first comparison of GFED burned area data with a preliminary version of the European Space Agency (ESA) Climate Change Initiative (CCI) burned area product was made.

The annual global fire emission estimates compared well between GFAS and GFED while FINN was structurally about 30% lower. Regionally, differences between GFAS and GFED can also be substantial. Some differences reflect the characteristics of different fire observation products used in the inventories:

1. Due to the higher sensitivity of active fire detection compared to burned area retrievals, GFAS[1] and FINN are able to account for smaller fires than GFED. This leads to substantial differences of emission estimates in regions where agricultural waste burning and other small fires are an important fire emissions sources such as in Europe, SE US, Central America, SE Asia.

2. While the FRP method theoretically eliminates the need for independent estimates of fuel load and combustion efficiency, previous studies (Heil et al., 2010) have found substantial variations in the conversion factor that is needed to derive the biomass combustion rate from the observed FRP. GFAS v1.0 therefore uses biome-specific conversion factors, which were derived from a multi-annual fit to GFED estimates. Even though the largest differences are found between biomes, the present study also reveals substantial variations within individual biomes. This includes mostly Africa and Australia where the savanna biome represents a range from dense woodlands to dry grasslands.

3. Preliminary burned area estimates from the ESA Fire CCI project are substantially higher than those used in GFED, which could indicate a low bias of GFED emission estimates and thus also GFAS.

4. The treatment of peat fires differs among the three inventories, and this is reflected in differences in the estimated carbon monoxide[2] emissions of up to 10 Tg/year globally.

[1] Note that the FRP algorithm (Wooster et al., 2006) uses active fire detection as a first step.

[2] Estimation of dry matter burned is particularly inaccurate for peat fires. Additionally, carbon monoxide emission factors are about twice as high as those from tropical and extra-tropical forests (Christian et al., 2003).

Validation of GFAS was mostly done by synthesizing recent literature focusing on atmospheric top-down constraints (i.e. inverse modeling) of emissions estimates. It was both done for well-studied individual fire events and for large-scale assessments focusing on continental-scale emissions estimates. We found that:

1. GFAS generally showed good skill in estimating the magnitude and timing of fire emissions. Uncertainties appear to be typically around 30%, and larger for exotic species. A tendency to underestimate appears in several fine-scale detailed investigations, but overestimation is also being reported in several cases.
2. In the boreal region, GFAS estimates were generally low, which could be related to the omission of part of the peat fires, or the omission of small fires in GFED. Both issues are being addressed in ongoing development of GFAS and GFED. Over Africa, GFAS agreed well with several validation studies but was somewhat low compared to inverse modeling studies.
3. The consequences of independent emission estimation studies for GFAS were not always straightforward because various studies often showed different results for the same event.
4. Some studies also yielded conflicting results in that large discrepancies were found for some trace gases, while the same study indicated that in the same fire event other trace gases compared well between models and observations. This points to uncertainties in our understanding of atmospheric chemistry and emission factors which translate biomass burned into trace gases or aerosol emissions.

A number of aspects were highlighted, on which future developments should concentrate:

1. Conversion factors that relate FRP with dry matter burned should be updated to include variations in the conversion factors caused by fire characteristics that are known *a priori* or observed. When relating GFAS FRP to GFED dry matter burned, the characteristics of the active fire and burned area observations have to be corrected.
2. The spatial distribution of peat fires should be better represented by including an updated peat map.
3. There is a need for a better spatial distribution and more homogeneous approach of validation studies, for example following based on a model inter-comparison study. However, this would require a large community effort.
4. Some emission factors, especially for rare species, are still quite uncertain. They should be updated when new information becomes available. In addition, satellite monitoring of fire plumes is starting to yield information on emission factors which should be included.
5. The absence of information on injection heights and the expected evolution of fires for 5 days into the future causes major inaccuracies in the atmospheric composition and air quality forecasts of MACC-II. It is recommended to extend GFAS with this information.
6. In order to provide operational resilience, the bias between daily FRP estimates from the two MODIS instruments should be explicitly characterized and removed in GFAS, and observations from VIIRS, MSG and the GOES satellites should be assimilated. The latter will require resolving the diurnal cycle and correcting the biases between and within the various FRP products.

Table of contents

1 Introduction

MACC-II (Monitoring Atmospheric Composition and Climate - Interim Implementation) is a European collaboration to produce global forecasts of atmospheric chemical composition and their reanalysis since 2003 as well as European forecasts of air quality. An important source of atmospheric trace gases and aerosol is the combustion of organic matter. The Global Fire Assimilation System (GFAS; Kaiser et al., 2012) – developed during the predecessor project MACC – produces near real time estimates of fire emissions and is used to provide input for atmospheric models in the MACC-II project and in the wider scientific and operational communities. GFAS is based on fire radiative power (FRP) as observed by the Moderate Resolution Imaging Spectroradiometer (MODIS) instruments aboard the Terra and Aqua satellites. Dry matter burned (DMb) is estimated from FRP using biome specific conversion factors based on DMb estimates of the Global Fire Emissions Database (GFED) version 3.1 (van der Werf et al., 2010). Finally, DMb is linearly transformed into emission fluxes of 40 smoke constituents using emission factors derived from field measurements (Andreae and Merlet, 2001; updated annually by M.O. Andreae; personal communication, 2012).

This document provides a quality assessment of the GFASv1 product, followed by recommendations on future product developments. Direct validation of fire emissions is difficult and most of the work described here is based on (*i*) comparisons with other products of emissions or parameters such as burned area and fuel consumption which are key for emissions calculations (Sections 2 and 3) and (*ii*) synthesizing the literature that used atmospheric top-down constraints in combination with atmospheric transport models to test how well atmospheric measurements are reproduced during specific fire episodes or on a monthly basis (Section 4). Next, several GFAS design features and their implications for the GFAS emission estimates are discussed in section 5. The last section of the report (Section 6) contains recommendations. Finally, a technical description of the GFAS software setup for the operational processing is provided in Annex B.

2 Inter-comparison of global inventories

We compare three emission inventories: GFAS v1.0 (Kaiser et al., 2012), GFED v3.1 (van der Werf et al., 2010), and FINN v1 (Wiedinmyer et al., 2006; 2011), both on global and regional scales. Here we focus on CO emissions because fires are a major source of CO, and because CO concentrations can be successfully monitored from space (Edwards et al., 2004). CO has an intermediate lifetime (weeks to months), which makes it ideally suited to detect fresh emission plumes (large enough tracer gradients) and long-range transport events (the lifetime roughly matches the time scale for intra-hemispheric transport). Most top-down emission estimates using inverse modeling techniques are based on CO observations (Section 4). The emission factors of other trace gases are frequently derived from their observed excess mixing ratios normalized to the one of CO (e.g. Akagi et al., 2011). Therefore emission estimates of many trace gases are closely related to the estimates from CO, and the main findings are likely to be applicable for several other species, too. Comparison of the inventories is made over the full period during which the products overlap (2003 – 2011), for 14 selected geographical regions and 7 biomes associated with dominant fire types of GFED3.1 (Figure 2.1). In addition, fuel consumption as calculated by GFAS and GFED are compared to field measurements derived from a literature survey.

This chapter starts with a description of the three emission inventories (Section 2.1), followed by the results of the inter-comparison (Section 2.2), a discussion (Section 2.3) and conclusions/ recommendations (Section 2.4). The main focus will be on differences related to using active fires or fire radiative power (FRP; GFAS and FINN) versus burned area (GFED) as primary source of fire data. In addition, we will look into the differences that result from using emission factors mostly from Andreae and Merlet (2001; GFAS and GFED) versus those from Akagi et al. (2011; FINN).

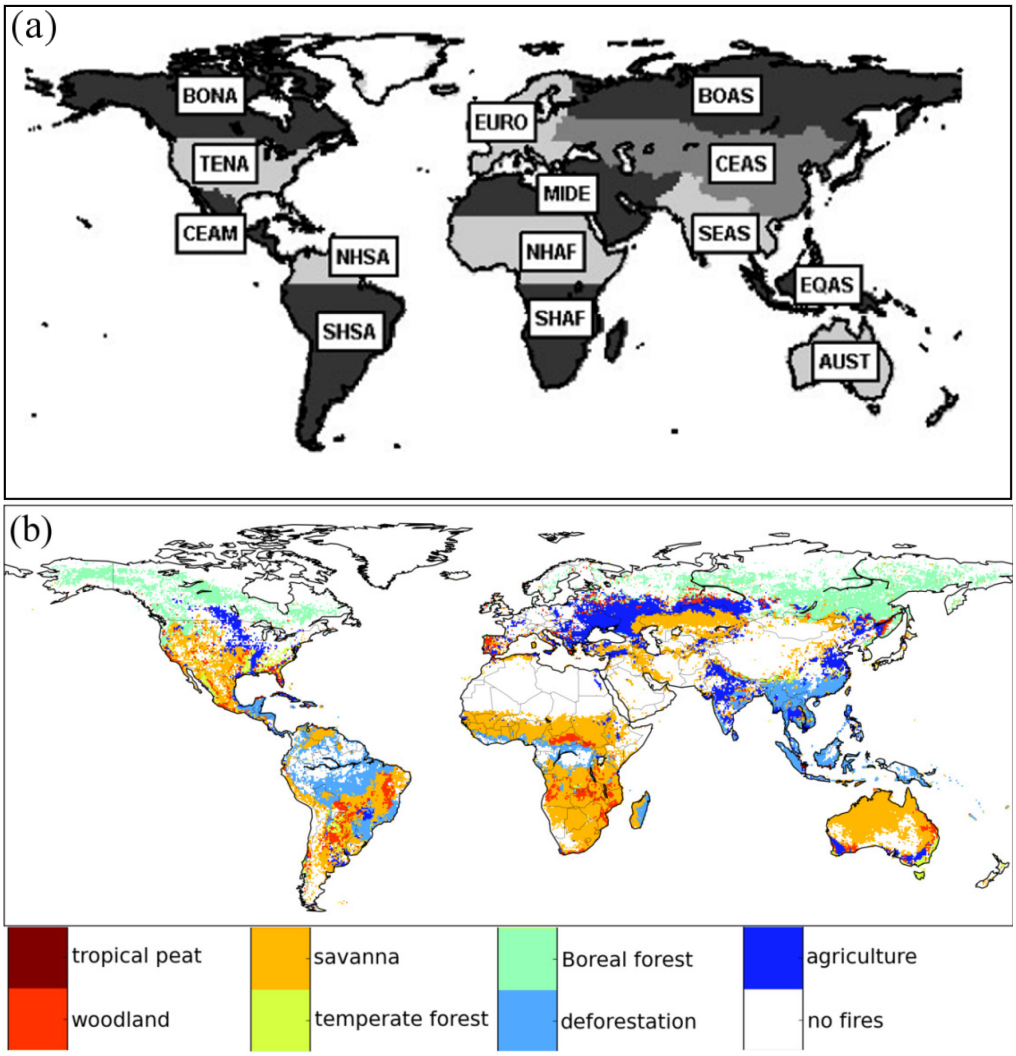

Figure 2.1: Geographical regions and biomes associated with fire type, used to stratify results. Panel (a) shows the 14 regions used for regional comparisons; and panel (b) the land cover types, based on the dominant fire type in GFED3.1. Abbreviations in panel (a) stand for Boreal North America (BONA), Temperate North America (TENA), Central America (CEAM), Northern Hemisphere South America (NHSA), Southern Hemisphere South America (SHSA), Europe (EURO), Middle East (MIDE), Northern Hemisphere Africa (NHAF), Southern Hemisphere Africa (SHAF), Boreal Asia (BOAS), Central Asia (CEAS), Southeast Asia (SEAS), Equatorial Asia (EQAS) and Australia and New Zealand (AUST), respectively.

2.1 Datasets

Here, a short description of the three emission inventories used in this report is given. Detailed methods of GFASv1 are provided by Kaiser et al. (2012), for GFEDv3.1 by van der Werf et al. (2010) and for FINNv1 by Wiedinmyer et al. (2006, 2011). In the remainder of the text we will omit the version numbers and refer to the inventories as GFAS, GFED, and FINN, respectively. If other versions are mentioned the version number will be explicitly stated.

2.1.1 *GFASv1*

The GFAS emission inventory provides daily global emission estimates at 0.5°×0.5° (GFASv1.0) and 0.1°×0.1° (GFASv1.1) resolution. It is based on NASA products from the MODIS instrument: FRP is extracted from MOD14 and MYD14, and geo-location from MOD03 and MYD03. Global FRP fields are derived from the satellite observations and corrected for partial cloud-cover, and observation gaps. Spurious signals from volcanoes, gas flares and other industrial activity are masked out by static blacklists which are updated regularly. Subsequently, FRP is converted to the combustion rate of dry matter with ecosystem-dependent conversion factors that are based on a previous intercomparison with GFED (Heil et al., 2010). The dry matter combustion rate is then scaled linearly to derive constituent fluxes of 40 trace gas and aerosol ingredients of smoke. Emission factors are taken from Andreae and Merlet (2001) with updates (M.O. Andreae, personal communication, 2012). In a final step, the total carbon emission flux is calculated from the fluxes of CO_2, CO, CH_4, BC and OC.

2.1.2 *GFEDv3.1*

The GFED database was developed when fire processes were included in the global biogeochemical Carnegie-Ames-Stanford-Approach (CASA; Potter et al., 1993) model, which simulates the exchange of carbon between the terrestrial vegetation and atmosphere. The main fire-related input dataset is burned area which is in version 3 derived from MODIS 500-meter burned area maps (Giglio et al., 2010) aggregated to 0.5°×0.5° resolution for the period of overlap with GFAS. CASA predicts biomass stocks and the burned area is used to estimate how much of the biomass is subject to fire. The combustion completeness is calculated within the model based on meteorological conditions. Finally, emission factors of Andreae and Merlet (2001) with annual updates are used to convert lost biomass into emissions of trace gases and aerosols.

2.1.3 *FINNv1*

The FINN emission inventory provides daily, 1 km resolution estimates of global fire emissions both for trace gases and aerosols. Emissions are calculated using:

$$E_i = A_{x,t} * B_x * FB * EF_i \quad (1)$$

Where E_i is the emission of species i, $A_{x,t}$ the area burned at location x and moment t, B_x the biomass loading, FB the fraction biomass burned and EF_i the emission factor. Like GFAS, FINN uses active fire observations from the MODIS Terra and Aqua satellite. However, in the case of FINN these observations are used to estimate burned area rather than FRP. Additionally FINN uses the MODIS land cover (IGBP classification) and the MODIS Vegetation Continuous Fields (VCF) products in its algorithm. The latter indicates the fraction of woody and non woody vegetation cover, and bare ground. Following Wiedinmyer et al. (2006) and Al-Saadi et al. (2008), for most land cover classes it

was assumed that each fire count corresponds to a burned area of 1 km^2, except for grasslands and savanna where it was assumed that each fire count corresponds to a burned area of 0.75 km^2. If the pixel with the fire observation was partly covered by bare area, this percentage was deducted from the burned area (e.g., a fire observation in a pixel with 50% bare ground would result in a burned area of 0.5 km^2). Fuel or biomass loading (*B*) was assumed to be land cover specific and estimates from Hoelzemann et al. (2004) were used, with a few updates as described by Wiedinmyer et al. (2011). The fraction of biomass burned (*FB*) was assumed to be related to the woody vegetation cover based on relations found by Ito and Penner (2004) and are further described by Wiedinmyer et al. (2006, 2011). Emission factors (*EF*) from the literature survey of Akagi et al. (2011) are used. For a complete overview we refer the reader to Table 2 of Wiedinmyer et al. (2011). In this report we used FINN data (MOZART 4 speciation) as available from http://bai.acd.ucar.edu/Data/fire/ (downloaded in January 2013).

2.2 Results

2.2.1 *Annual mean CO emissions*

Figure 2.2 shows mean annual CO emissions calculated by the different inventories. The three inventories show similar global patterns but on a regional scale they diverge. Important biomass burning regions include boreal forests with a heterogeneous fire landscape, deforestation areas of South America (especially Amazonia), African savannas (with highest emissions occurring in regions of higher biomass production closer to the equator), Southeast Asia including Indonesia, and Northern Australia. Figure 2.3 shows the differences in mean annual CO emissions between the different inventories. In boreal North America GFED generally estimates larger CO emissions than GFAS, although for individual fires the opposite is occasionally observed. Over the US and Central America GFAS is generally higher than GFED. South America shows a mixed picture where GFAS is higher than GFED for some regions while in others GFED is higher. In Africa GFED emission estimates are usually higher than GFAS, especially over areas of high annual emissions. In boreal Asia, for some regions or events GFAS is higher than GFED and for other regions it is the other way around. In Southeast Asia GFAS is somewhat higher than GFED but not for all regions and in equatorial Asia a mixed pattern was observed where depending on the event GFAS estimates might be larger or smaller than GFED estimates. Finally, for Australia GFED was larger for northern Australia with relatively high rainfall rates while GFAS estimates were larger for dryer parts of central Australia. Similar differences were observed between GFAS and FINN (Figure 2.3b) and GFED and FINN (Figure 2.3c), where GFED and FINN were most different.

Figure 2.4 shows mean CO emissions calculated by GFAS divided by the sum of the mean GFAS and GFED emissions to indicate the relative difference instead of the absolute values as shown in Figure 2.3. This results in a map where: (*i*) zero indicates GFAS predict zero emissions but GFED does predict emissions, (*ii*) '0.5' indicates that calculated GFAS emissions are equal to GFED emissions and (*iii*) one indicates that calculated GFAS emissions were observed but GFED showed zero emissions over the study period. GFAS shows emissions in many regions of low fire intensity where GFED doesn't have emissions. For dry savannas and agricultural areas GFAS is usually higher than GFED, while for more intensely burning savannas and agricultural areas it is the other way around (compare Figure 2.1 with Figure 2.4). In most deforestation areas and boreal forests (e.g., most of

Amazonia, boreal North America) GFED shows higher emissions than GFAS, while GFAS predicts higher estimates elsewhere (e.g., most of Southeast Asia).

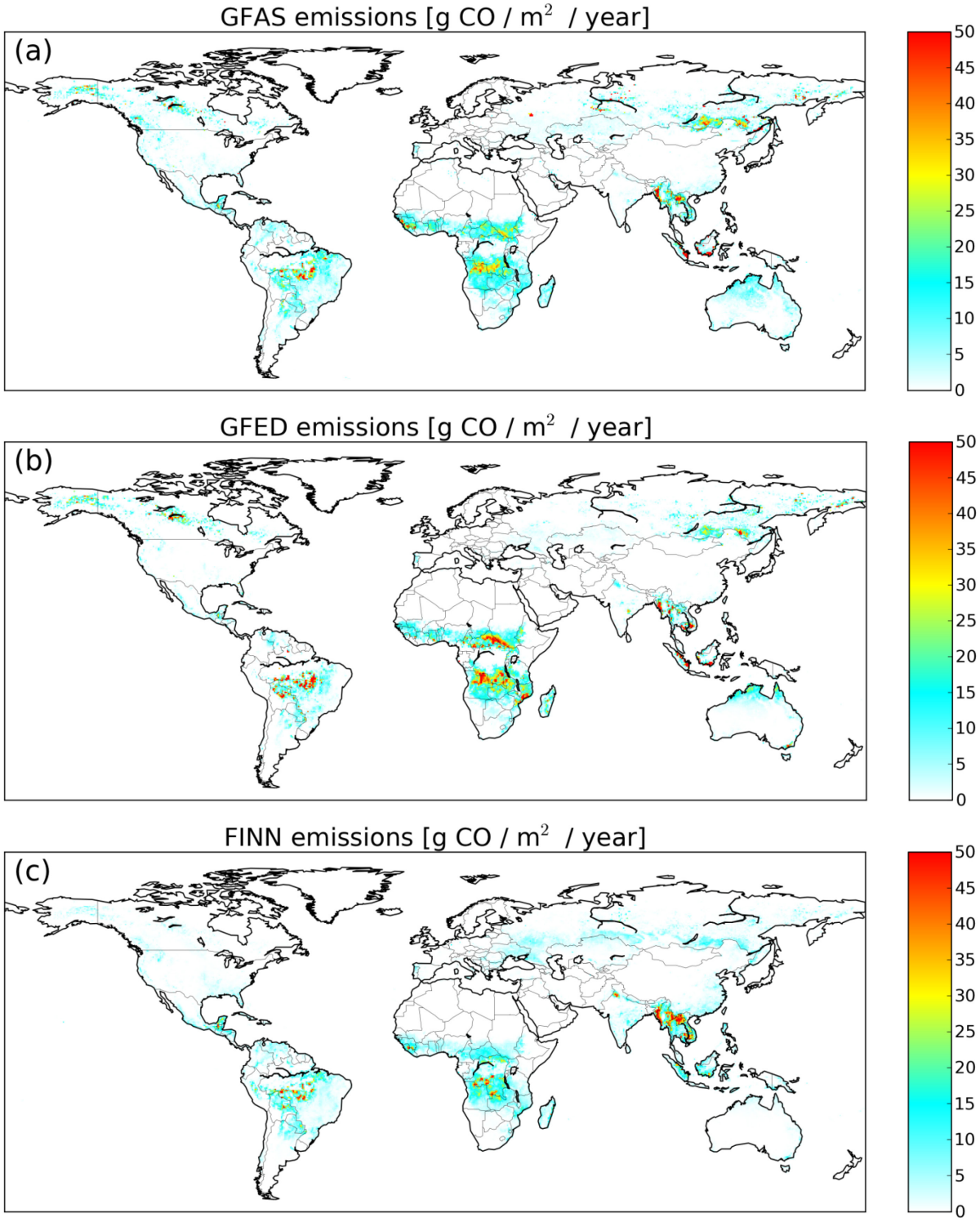

Figure 2.2: Mean annual CO emissions [g CO m^{-2} yr^{-1}] for 2003 until 2011. The different panels show the results of GFAS (a), GFED (b), and FINN (c).

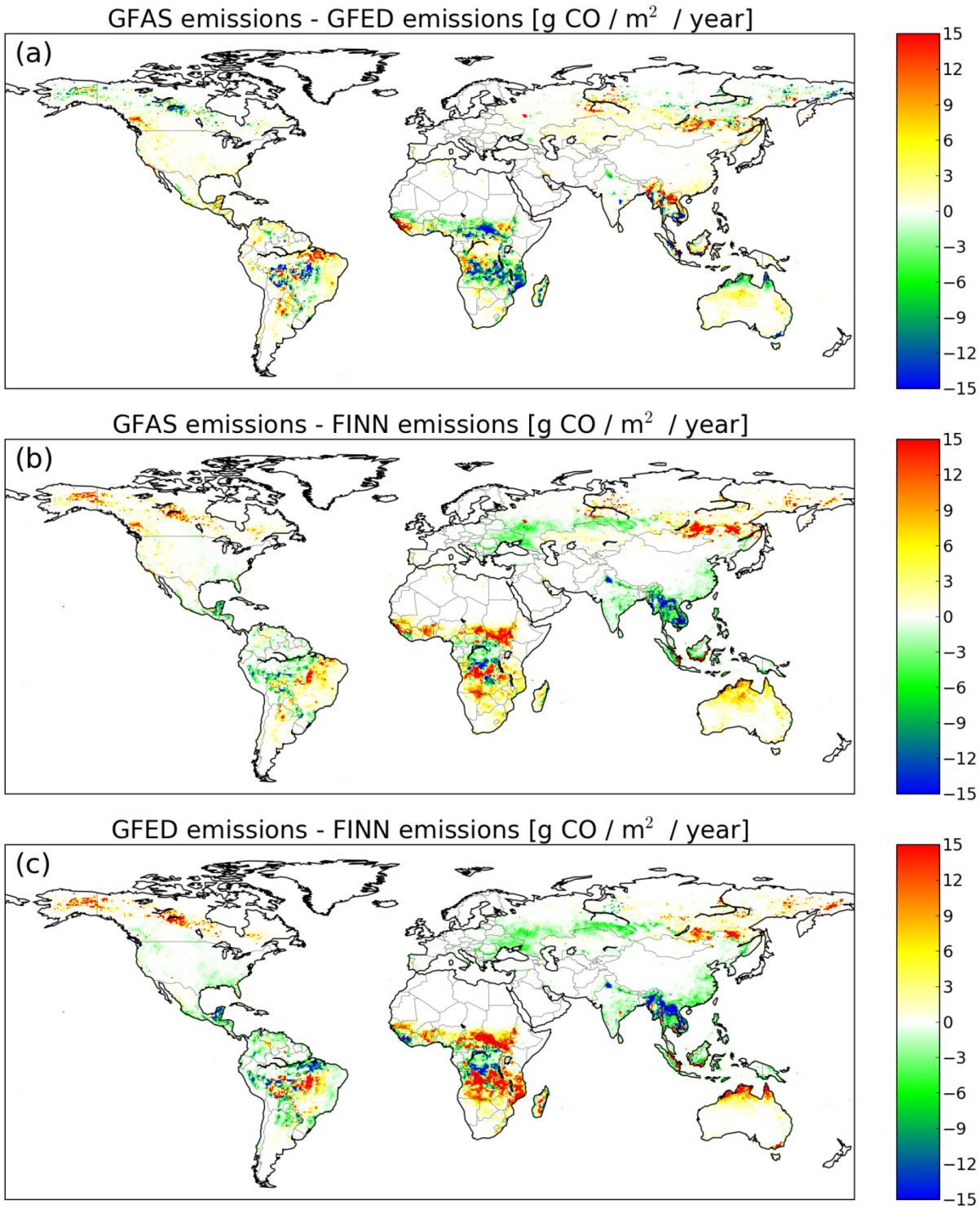

Figure 2.3: Difference in predicted annual mean emissions between GFAS, GFED and FINN [g CO m^{-2} yr^{-1}] for 2003 until 2011. Panel (a) shows the difference between GFAS and GFED; Panel (b) between GFAS and FINN; and panel (c) between GFED and FINN.

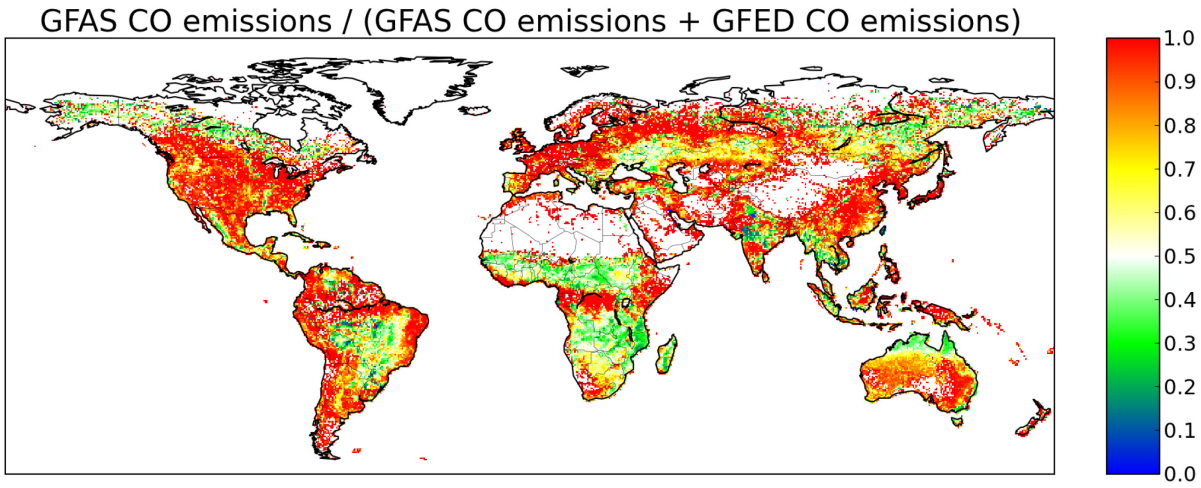

Figure 2.4: Ratio of GFAS / (GFED + GFAS) CO emissions. A value of 0.5 (white) indicates that both products predict equal emissions.

2.2.2 *Temporal variability in CO emissions*

Seasonal mean variations in CO emissions as calculated by GFAS, GFED and FINN are shown in Figure 2.5. In boreal North America GFAS and GFED emissions are considerably higher than FINN emissions with GFAS slightly lower than GFED. In temporal North America, Central America and the northern half of South America, GFAS and FINN are higher than GFED. GFAS and GFED agree very well over Europe with FINN showing higher emissions. In the Middle East GFAS showed higher emissions than GFED and FINN which agree well over the region. Both northern and southern Africa show a good agreement between GFAS and FINN, while GFED showed higher emissions, especially in November, December and January for northern hemisphere Africa and June, August and September for southern hemisphere Africa. In boreal Asia all three inventories showed quite different patterns, FINN showed clearly lower emissions than GFAS and GFED. Estimated emissions for Central Asia and Southeast Asia were highest in FINN and considerably lower for GFAS and GFED; while equatorial Asia and Australia showed relatively low emission estimates by FINN and good comparison between GFAS and GFED. Overall differences between GFED and FINN are largest while GFAS has characteristics of both other inventories. Globally GFAS and FINN show higher estimates for the months February, March, April and May while GFED has higher estimates for the months July, August and September.

In order to elucidate the reasons for the differences between the emission inventories, a seasonal characterization (like Figure 2.5) was also made for different biomes (Figure 2.6). For several biomes two annual peaks are observed. During summer, fires occur in temperate regions and higher latitudes, while tropical fires occur during the winter. For agricultural regions, emission estimates were considerably higher for FINN than for GFAS and GFED, being relatively similar. In case of the fires associated with deforestation, estimated emissions by FINN were relatively high for the northern hemisphere winter (tropical dry season) and high GFED emission estimates were observed for the southern hemisphere winter. GFED emission estimates were high compared to FINN for large parts of the Amazon, while FINN emission estimates were higher for Southeast Asia and Central America.

Although seasonal patterns in the three inventories were similar for boreal forests, actual estimated emissions were quite different. Estimated emissions from GFAS were somewhat lower than GFED, but several times larger than FINN. In temperate forest estimated FINN emissions are higher than GFAS and GFED, especially early in the year (February, March, April and May). Savanna fire emissions showed good comparison between GFAS and GFED, and lower estimates by FINN. For woodland fires on the other hand GFAS and FINN were relatively similar while GFED showed higher values, especially for fires occurring in August and September. Good agreement was found between GFAS and GFED for tropical peat fire emissions, while FINN estimates were several times lower.

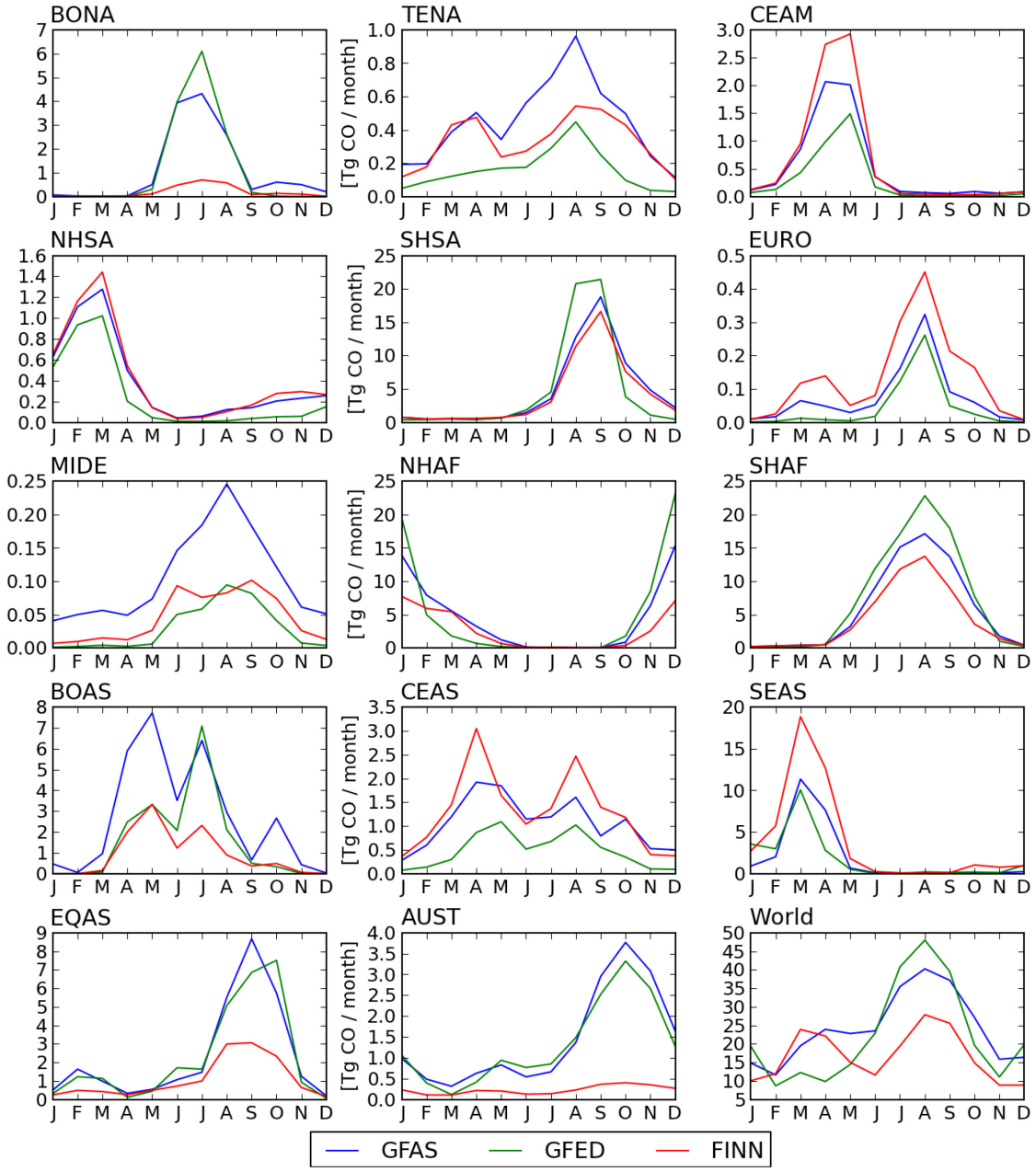

Figure 2.5: Mean seasonal CO emissions for 14 selected regions (see Figure 2.1a) and the world for 2003 until 2011. Emissions are shown for three different fire emission inventories: GFAS, GFED and FINN.

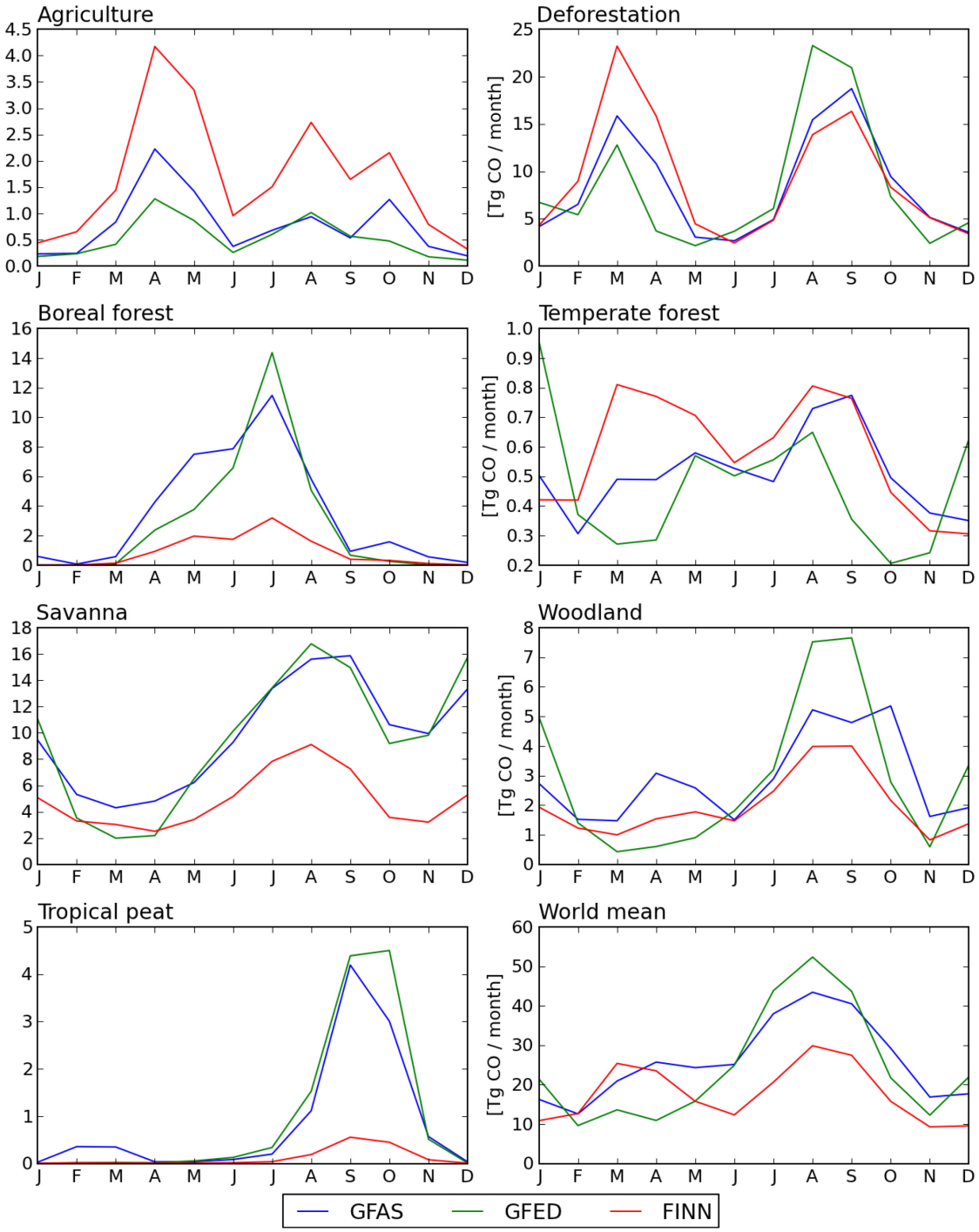

Figure 2.6: Mean seasonal CO emissions for 7 biomes associated with dominant fire type in GFED (see Figure 2.1b) and the world for 2003 until 2011. Emissions are shown for three different fire emission inventories: GFAS, GFED and FINN.

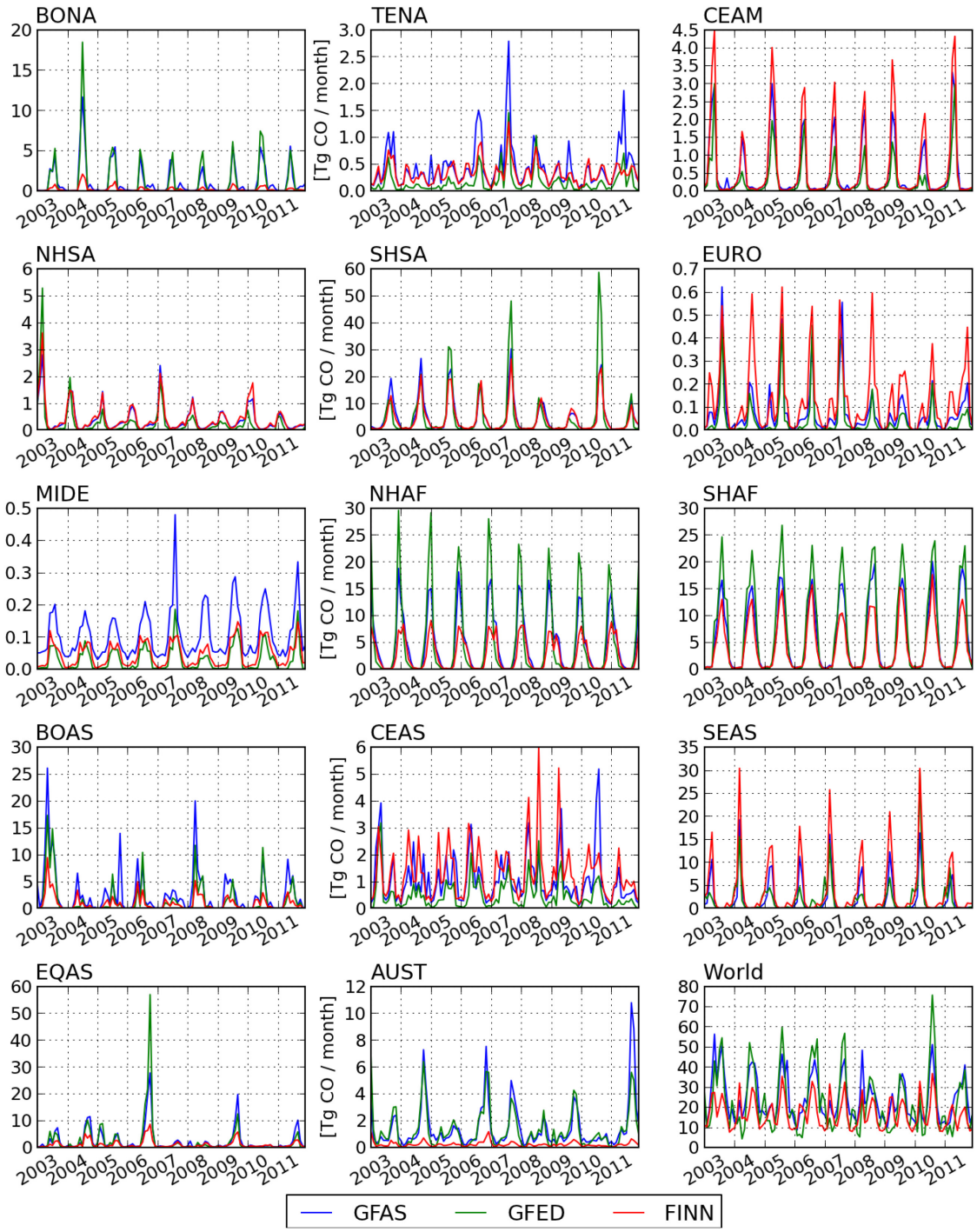

Figure 2.7: Inter-annual variation in CO emissions for 14 selected regions (see Figure 2.1a) and the world between 2003 and 2011. Emissions are shown for three different fire emission inventories: GFAS, GFED and FINN.

Inter-annual variations in CO emissions are shown for selected regions and globally in Figure 2.7. Results were similar to the seasonal results, with some inventories having consistently higher emission estimates than others for the same regions as in Figure 2.4. There are a number of exceptions like temperate North America, southern hemisphere South America, Europe, Central Asia and equatorial Asia, where inventories showed agreement during some years but deviated in others. Also, some regions showed relatively constant emissions over the years (e.g., Africa), while in others mean emissions were affected by some extreme years (especially: temperate North America, boreal Asia and equatorial Asia).

2.2.3 *Fuel Consumption*

A comparison was made between fuel consumption calculated by GFAS and by GFED (Figure 2.8) and fuel consumption derived from the literature. Fuel consumption was calculated by dividing mean annual dry matter burned of GFAS and GFED by mean annual percentage burned area of GFED, for each grid cell and expressed in units of ton per hectare burned area. Although overall the fuel consumption maps of GFAS and GFED are quite similar, regional differences were observed. GFAS showed more spatial variability in fuel consumption resulting in some areas where GFAS estimates were higher than GFED (e.g., central Australia and the Amazon) and lower for others (e.g., East Africa and boreal forests). It is noticed that GFAS tends to have higher fuel consumption for areas of low burning intensity and GFED for areas of high burning intensity (i.e., high emissions). Areas with low annual burned area are often dominated by small fires, resulting in GFAS observing more fires than GFED. This can result in unrealistically high fuel consumption estimates for GFAS. To prevent this effect from seriously affecting the results of this comparison, areas with less than 0.1 percent annual burned area were masked out for this exercise.

A comparison of fuel consumption for several biomes as found in literature according to a literature survey where all peer-reviewed papers detailing fuel consumption were compiled to estimate biome-average fuel consumption estimates (Detmers and van der Werf, 2013) with fuel consumption estimated by GFAS and GFED is given in Table 2.1. Results were weighted for burned area to prevent pixels in regions with little fire occurrence from dominating the results. It is shown that (weighted) biome averages of both GFAS and GFED are on the high end for boreal forest, savanna, tropical peat and agricultural lands but they compared better with field studies in tropical forest, temperate forest and woodlands. For most biomes, GFAS had slightly higher fuel consumption values than GFED. Note that this comparison shows weighted biome averages compared to averages as found in literature; considerable regional uncertainty remains, as fuel consumption varies regionally within the biomes (Figure 2.8) and with literature studies not always well distributed over the biome (Figure A. 1).

Table 2.1: Fuel consumption [ton / ha burned area] per biome (Figure 2.1b); a comparison of literature derived values (from Detmers and van der Werf, 2013; numbers between brackets are standard deviations) and results of Figure 2.8. Results are weighted for burned area. Fuel consumption is calculated by dividing emissions by percentage burned area of GFED.

Biome	Literature	GFAS weighted mean	GFED weighted mean
Boreal forest	24 (16)	59.6	54.1
Tropical forest	81 (74)	68.8	57.5
Temperate forest	31 (51)	24.6	26.5
Woodland	12	13.2	12.6
Savanna	3.5 (1.7)	8.1	7.0
Tropical peat	150 (122)	330.3	258.1
Agriculture	4 (4)	7.8	7.6

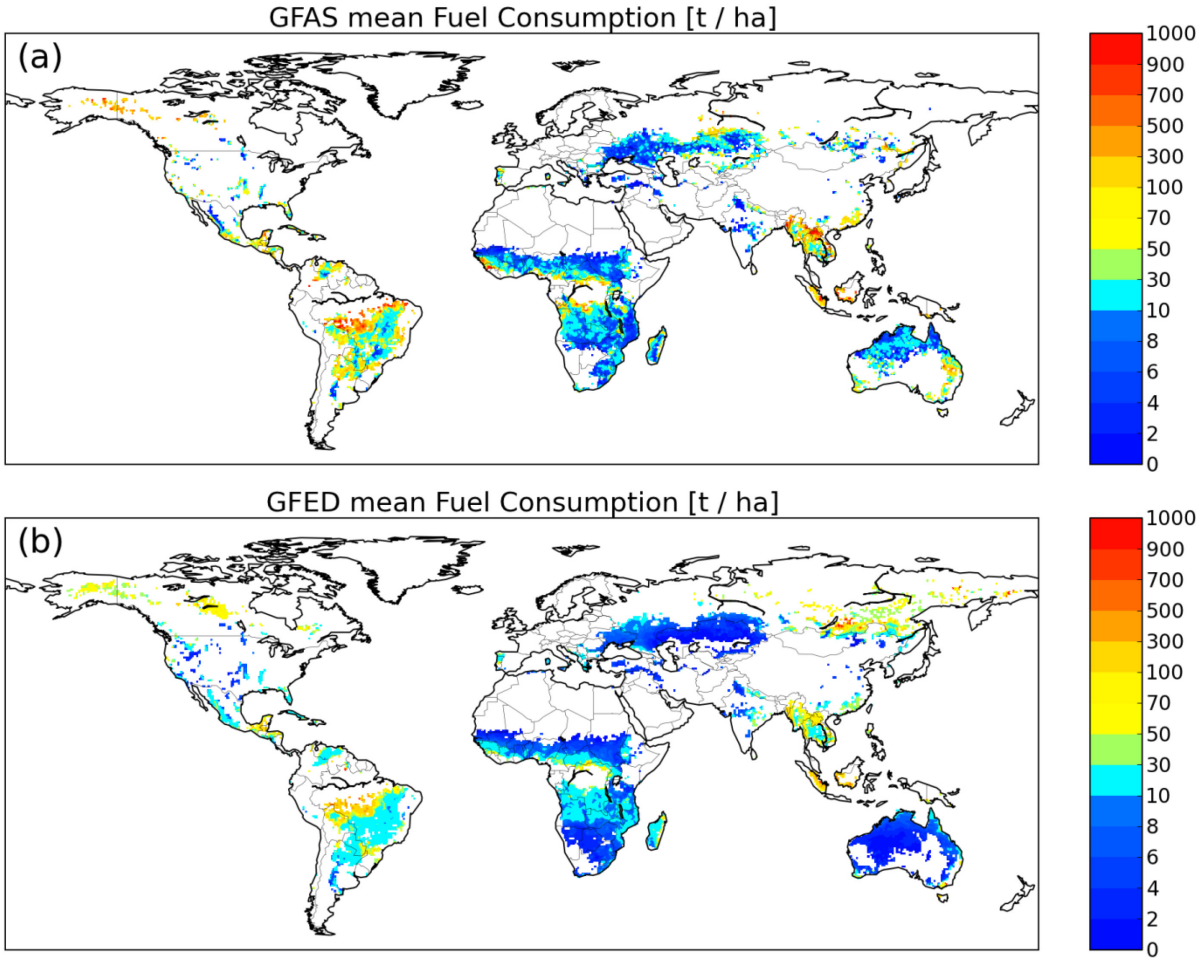

Figure 2.8: Global maps showing fuel consumption [ton / ha burned area]. Panel (a) shows GFAS fuel consumption; and panel (b) shows GFED fuel consumption. Fuel consumption is calculated by dividing emissions by percentage burned area of GFED.

2.3 Discussion

First the methodological differences between GFAS, GFED and FINN are discussed shortly (see Section 2.1 for a detailed product description), followed by a discussion of the differences between the products over 2003 – 2011. Of the three inventories, GFAS is unique in that it avoids the need for independent data on fuel loads and combustion efficiency. FINN is based on the same active fire data that is used to calculate the FRP for GFAS, but it uses the fire observations to estimate burned area from which biomass burned is derived using land cover type, vegetation continuous fields and relations found in literature. GFED is unique as it is based on a burned area product and fuel model in contrast to GFAS and FINN, which are based on active fire observations. FINN uses a static database for fuel load. A clear advantage of the active fire based inventories over GFED is that they are based on near real time observations and, in the case of GFAS, the fact that FRP is directly related to the biomass combustion rate (Wooster et al., 2005). Also, active fire based emission inventories include small fires that are not observed by GFED (smaller than ~100ha; Randerson et al., 2012). A clear advantage of burned area based products (GFED) is the fact that burning scars are often visible for many days and it can therefore observe fires that occurred in cloud covered areas, as long as cloud cover is not too persistent (Randerson et al., 2012). GFAS corrects for partial cloud cover during a single day by assuming a uniform distribution of fires in each grid cell. Observation gaps due to cloud cover are filled using the assumption of persistence from day to day. This assumption may lead to an overestimation when precipitation beneath the clouds quells the fire activity.

The emissions of different gasses are calculated using emission factors and dry matter burned, all emission inventories assume a static relation between dry matter burned and emissions of different chemical components. While GFAS and GFED rely on emission factors from the database of Andreae and Merlet (2001), FINN used the emission factor compilation of Akagi et al. (2011) with a few additions. Actual emission factors used for GFAS are given in Kaiser et al. (2012), for GFED in van der Werf et al. (2010), and for FINN in Wiedinmyer et al. (2011). Different emission factors are a potential source of differences between GFAS and GFED on the one hand, and FINN on the other. It is noted however that differences in emission factors are never the source of large deviation between the emission inventories, for GFAS for example the CO emission factors for savanna, tropical forest, and agriculture are 61, 101 and 92 g (CO) per kg dry matter burned, respectively; for GFED the CO emission factors for savanna, tropical forest, and agriculture are 61, 101, and 94 g (CO) per kg dry matter burned, respectively; and for FINN CO emission factors for savannas, evergreen broadleaf forest and croplands are 59, 92 and 111 g (CO) per kg dry matter burned, respectively.

2.3.1 *Annual mean CO emissions*

Globally it was shown that the three studied emission inventories identify the same global hotspots of biomass burning and fire emissions: African savannas, tropical deforestation zones of South America and Southeast Asia and some boreal regions where large fires occurred (Figure 2.2). Total annual global CO emissions of the three inventories are the same order of magnitude (GFAS: 288, GFED: 266, and FINN: 200 Tg CO yr^{-1}). However, regionally the different inventories show substantial differences. For many regions GFAS emission estimates are in between the estimates from GFED and FINN. This can be explained by GFAS being based on the same active fire satellite observations as FINN but conversion factors from FRP to dry matter combustion have been derived using GFED dry matter combustion rates for each biome individually (Kaiser et al., 2012). It seems that many local

differences between GFAS and GFED originate from the assumption that conversion factors should be constant for each biome. Heil et al. (2010) showed that in reality conversion factors vary between biomes, and also to a lesser degree within the biomes. Compared to GFED, this results in regional overestimation of GFAS emissions when actual conversion factors are below the biome average and underestimation when actual conversion factors are above the biome average. The fact that conversion factors are not stable over the biome is likely caused both by vegetation cover aspects (e.g., tree cover, leaf area index, vegetation moisture content) and differences between burned area and active fire products. It is also possible that there is a seasonal variation in the conversion factor, if, for example, the fuel moisture content varies with time. Giglio et al. (2005) noted that the number of fires observed per burned area varies widely across the globe.

In savanna regions (see Figure 2.1b), GFAS estimates higher emissions for areas with low burning intensity such as dry savannas; while GFED estimates higher emissions for high burning intensity including humid savannas. It seems that conversion factors for arid drylands are in general lower than for humid drylands, causing these local over- and underestimations relative to GFED. This can be explained by the fact that GFAS is more sensitive to small fires, occurring in dry areas where fuel loads are not sufficient for fires to spread over larger areas and be detected by the burned area algorithm. GFED on the other hand might observe cloud covered fires that occur during early season burning in the more humid African savannas. Another possible explanation could be differences in fuel characteristics, causing the relationship between FRP and DM-burned to vary spatially over the biome. Since GFAS has derived the relation between FRP and dry matter combustion rate from GFED over biomes as a whole, mean values for the entire biome are similar but GFAS emission estimates are higher for dry savannas and GFED for humid savannas (Figure 2.4). FINN emission estimates for savannas are lower than GFAS and GFED, with the largest temporal deviation found for peak burning season and the largest spatial deviation for humid savannas. It is noted that fire size is often largest in humid savannas during the peak burning season; fire characteristics are likely to be related to observed differences between burned area and active fire based inventories.

Although it is likely that for tropical deforestation zones the MODIS active fire product (GFAS and FINN) underestimates the fire occurrence because fires can be obscured by persistent cloud cover and overstory, the problem may be more severe for burned area estimates because they are not tuned to detect these fires which are often relatively small. Therefore, GFED used both active fire observation and burned area to estimate fire emissions in this biome. Active fire observations were used to calculate fire persistence (related to deforestation rate), combustion completeness and fire-induced tree mortality. Final emissions were estimated using the burned area product in combination with biomass density and deforestation rates using active fire persistence (for detailed methods, see van der Werf et al., 2010). This way, van der Werf et al. (2010) found relatively high fuel consumption for Southern and Central America, and lower fuel consumptions for Africa and Southeast Asia. These differences likely explain the relative high emissions observed by GFAS and GFED for the Southern Hemisphere and low observed emissions for the Northern Hemisphere compared to FINN. Moreover, GFED is based on burned area observations and might therefore miss small fires. This results in a relative high emission estimate of GFAS and FINN in some areas and for GFED in others. GFAS and FINN generally give higher estimates of emissions for Africa, southeast Asia and northern Brazil, while GFED gives higher estimates for central Amazonia. A possible explanation might be relative

cloud cover, where very cloudy areas might show higher emission estimates in GFED and areas with more clear skies in FINN. GFAS corrects for cloud cover by assuming the non-cloudy part of a pixel to be representative for the whole pixel and for completely cloud obscured pixels, GFAS assumes the fire observations are equal to the last observation. Another factor of influence might be the size of deforestation. GFED is tuned to capture large scale deforestation in central Brazil, but small scale deforestation in for example Africa and some regions in Southeast Asia might be better monitored using active fire products.

In agricultural areas the active fire product observes more fires than the burned area product. This results in GFAS and FINN having more fire observations over these areas compared to GFED. Therefore, the conversion factor used in GFAS might be on the low side, explaining the large difference between GFAS and FINN. It has to be mentioned that in FINN one fire count corresponds to 1 km^2 burned, but especially for those small agricultural fires which do not occur in burned area products, this assumption might overestimate agricultural burning by overestimating area burned.

In boreal forests GFAS and GFED emission estimates are considerably higher than FINN. The difference between GFED and FINN most likely arises from a difference in estimated burned area or biomass, as combustion completeness (~0.3 for woody vegetation) and emission factors are quite similar for both products (Wiedinmyer et al., 2011; van der Werf et al., 2010). The relative high conversion factor (i.e, 1.55; Kaiser et al., 2012) of GFAS and the low emission estimates of FINN for boreal forest suggest that burned area products may observe some fires that do not occur in active fire products, possibly due to cloud cover. Also here it seems that although the mean values from GFAS and GFED are similar; some, especially small fires might be more likely to be observed by GFAS while large fires could be better captured by GFED. Because the biome conversion factor is used to link GFAS and GFED, this results in some areas of higher emission estimates by GFAS while others show higher values in GFED. Fire size in boreal forests might for example be affected by proximity to cities or villages but also by physical features of the landscape like rivers and mountain ranges.

2.3.2 *Temporal variability in CO emissions*

The seasonality of CO emissions for different regions and land cover types provide new insights into differences between GFAS, GFED and FINN. In general, the seasonality as observed by the inventories is very similar and boosts confidence in the products. In the case of Europe for example, relative good agreement is found between the different emission inventories, with FINN being somewhat higher than GFAS and GFED that might underestimate emissions from early season (agricultural) fires (Figure 2.5). In general, it seems that differences in seasonality between the products can be explained in similar ways as differences in magnitude (see Section 2.3.1). There are however some notable exceptions, in the Middle East for example GFAS never drops to zero, indicating that gas flares may not have been masked out sufficiently in the region. Also, exceptionally low values of FINN occur over Australia. This is likely related to an underestimation of the burned area per pixel. One can expect that one fire count in Australian humid savannas corresponds to more than the 0.75km^2 assumed for grasslands and savannas in FINN, so that FINN underestimates the burned area (Giglio et al., 2005).

Differences in seasonality for different biomes provide information on the performance of the different inventories for different fire types and weather conditions. In the case of agricultural fires differences might arrive from a relative large share of small fires that are not observed by burned area products and therefore lead to an underestimation by GFED. Due to the scaling of GFAS FRP to DMb conversion factors to GFED data, GFAS will also underestimate these emissions, while FINN likely overestimates burned area by assuming an unrealistically large value of 1 km^2 per burned pixel in agricultural areas. Globally, GFAS and FINN estimate higher emissions early in the year (coinciding with the burning season of the northern hemisphere tropics), while GFED is higher later in the year (with fires occurring in the southern hemisphere tropics and northern hemisphere temperate and boreal regions). These higher emission estimates of GFAS and FINN (early in the year) compared to GFED are observed for several biomes (see Figure 2.6). As it occurs both in GFAS and FINN, it is likely that the difference is related to the use of the active fire product versus the burned area product that is input to GFED. A particularly large difference is found for tropical peatland, where GFAS and GFED show high annual emissions and FINN does not; this is because peatlands in Indonesia and Malaysian Borneo have been included separately into the GFAS and GFED biome map (van der Werf et al., 2010), while they have not been especially accounted for in FINN.

In most regions inter-annual variations are as expected, with the same relationship between GFAS, GFED and FINN in all years. A good example is Africa (both hemispheres), where there is variation over the years, but GFED estimates are always higher than GFAS which is again higher than FINN. There are also regions where emission estimates agree for some years but deviate in others, those are more complicated cases that need individual discussion. In the case of Europe for example, good agreement is found for 2003, 2005, 2006 and 2007; but FINN shows considerably higher estimates than GFAS and GFED for 2004 and 2008. It is expected that during those years more, but relative small fires occurred. As FINN is based on the active fire product, a high emission estimate indicates high fire count; GFAS however is based on the FRP of the same product, therefore a peak solely observed in FINN but not in GFAS indicates FRP should have been relatively low for those events (i.e., small fires). Another example of specific deviation in one particular year is Australia: while there is good agreement between GFAS and GFED during most years, 2011 forms an exception. The 2011 la Niña event caused northern Australia (where most fires occur) to receive more rainfall than normal; it is possible that during these events the conversion factor used to link GFAS and GFED is not realistic as fire characteristics (size, temperature, fuel load, fuel moisture, etc.) might be different during or after such an event.

2.3.3 *Fuel Consumption*

Although there is good global agreement between GFAS and GFED fuel consumption estimates, local differences are observed (see Figure 2.8). Although the conversion factors used by GFAS result in similar mean fuel consumption, the spatial distribution of active fire observations and burned area are not equal as both products have their own strengths and limitations. The estimated fuel consumptions of GFAS and GFED are compared to field measurements (Table 2.1). Good agreement is found for deforestation, temperate forest and woodlands. Fuel consumption for agricultural regions are on the high end in both products. However, on a global scale it seems likely that emissions from agricultural fires might still be underestimated as the burned area product is not sensitive to these relatively small fires. Fuel consumption estimated by GFED might be representative for relatively large agricultural

fires but less so for small agricultural fires, as they were not observed. Boreal forest fuel consumption estimates are also high, possibly caused by errors in the estimates of biomass or combustion factors used in GFED. Savanna fuel consumption estimates are also higher than observed during measurements, presumably because most of those measurements have been carried out in relatively dry savannas/grasslands (see Figure A. 1.). Combustion factors of savanna are more certain than those of forests as fine fuels usually burn completely, therefore this is not expected to cause large errors in this case (van der Werf et al., 2010). In the case of tropical peatlands large uncertainty exists both in field measurements (with a standard deviation of 122 ton/ha) as in the emission inventories (van der Werf et al., 2010).

2.4 Conclusions

During the development of GFAS a major emphasis was placed on consistency with GFED by including biome-specific conversion factors. This chapter shows this has been achieved over large scales with regard to absolute emissions and that the various products indicate roughly the same seasonality. On a regional scale GFAS and GFED do deviate in absolute emission estimates. This does not necessarily indicate that GFAS has to be adjusted, as GFED is known to have difficulties in detecting small fires such as those occurring in agricultural areas.

For the next GFAS version, the values of the conversion factors should be carefully reconsidered, taking gradients in fire characteristics and differences between burned area based and active fire based products into account. The challenge will be to combine the strengths of GFAS (for example the superior detection capability of small fires) with those of GFED related to a better representation of fire processes within biomes dominated by large scale burning. In FINN the assumptions on the relation between fire count and burned area may be oversimplified causing regionally dependent over- or underestimations (Giglio et al., 2005).

For some biomes better agreement is found between the three global emission inventories than for others. In some cases, a clear explanation is found and in the future the emerging issues can be addressed. If we make the assumption that good agreement between the various inventories indicate smaller absolute errors, then emission estimates are more accurate for savanna, woodland, and deforestation areas while the estimates for agricultural land and tropical peat areas need improvement. Agricultural lands are a particular case, because the fire regime there is dominated by relatively small fires. Currently GFED does not include such small fires due to the missing sensitivity of the underlying burned area product. As a result, emissions in such regions are underestimated in both GFED and GFAS, because of the ecosystem-dependent conversion factors in GFAS which were scaled to GFED results. Another land cover class with high uncertainties is peat, of which both the spatial extent and the emission factors are poorly known. Peat fires are responsible for considerable emissions close to densely populated areas in the tropics, and failure to classify peat fires as such might cause considerable underestimation of emissions (Figure 2.6).

A new version of GFED is currently in preparation and will include smaller fires by using the MODIS active fire product to estimate additional burned area that is not observed by the burned area product (Randerson et al., 2012). It is recommended to update the GFAS FRP to DMb conversion factors based on this new GFED version. This should then lead to a quality improvement of GFAS in regions dominated by small fires (e.g., agricultural regions).

3 Inter-comparison of GFAS FRP with ESA CCI burned area

GFAS fire radiative power (GFAS_FRP) and dry matter combustion rates (GFAS_DM) were compared with burned area estimates for 10 selected test sites from the ESA Fire CCI merged burned area product (denoted here as CCI_BA) (Table 3.1). The ESA Fire CCI project (www.esa-fire.cci.org), which is part of the Climate Change Initiative (CCI) of the European Space Agency (ESA), focuses on the development of long time series of burned area constructed from European multi-sensor satellite data. The satellite sensors comprise the Along-Track Scanning Radiometer (ATSR), SPOT VEGETATION (VGT) and Medium Resolution Imaging Spectrometer (MERIS). For the comparison with GFAS, we use and present here the preliminary 0.5 degree gridded, merged, monthly burned area product, which was provided to us in February 2013. As additional products, GFED3 and GFED4 burned area and GFED3 DM estimates are included in the comparison.

Table 3.1: Characteristics of the ESA Fire CCI burned area test sites.

Site	Region	Main ecosystem characteristics	xsize (number of grid cells)	ysize (number of grid cells)	longitude bounds	latitude bounds	area of the domain [km^2]
SS01	Canada	Boreal forest with some peat	5	17	-111.5, -109.0	53.5, 62.0	140,000
SS02	Colombia	Savanna with some forest	9	9	-72.0, -67.5	3.5, 8.0	249,000
SS03	Brazil	Tropical forest with some savanna	9	9	-51.5, -47.0	-11.5, -7.0	247,000
SS04	Portugal	Mixture of savanna with forest	7	12	-9.5, -6.0	38.5, 44.5	194,000
SS05	Angola	Savanna with some forest	9	9	13.5, 18.0	-10.5, -6.0	248,000
SS06	South Africa	Savanna with some forest	9	10	27.5, 32.0	-27.0, -22.0	253,000
SS07	Kazakhstan	Savanna with some agriculture	6	14	53.0, 56.0	46.5, 53.5	167,000
SS08	Borneo	Tropical forest with peat	9	9	111.5, 116.0	-4.0, 0.5	250,000
SS09	Russia	Boreal forest with some peat	6	16	109.5, 112.5	50.0, 58.0	174,000
SS10	Australia	Savanna	9	10	130.0, 134.5	-17.5, -12.5	269,000

3.1 Comparison of mean annual totals

The summary statistics computed for each test site (Table 3.2) show that mean annual total area burned in the merged ESA Fire CCI burned area product (CCI_BA) is 1.4 to 5.8 times higher than the GFED3 burned area estimates (GFED3_BA). Integrated over all test sites, CCI_BA is 2.5 times higher than GFED3_BA. GFED4_BA and GFED3_BA are within 15%. As expected, the site-averaged conversion factors (CF) calculated from the GFAS_FRP and GFAS_DM data (CF_GFAS) reflect the burned-area weighted contribution of the fuel-type specific conversion factors, with high values occurring at the sites SS01 (Canada) and SS09 (Russia), where mostly EFOS (extratropical forest with potential burning of duff/peaty soil material[3]) burned and SS08 (Borneo; Table 3.3).

Table 3.2: Summary statistics for the ESA fire CCI test sites covering the years 2003 to 2009. CF_GFAS denotes the conversion factor calculated from dividing GFAS_DM by GFAS_FRP. CF_GFED denotes the derived conversion factor calculated from dividing GFED3_DM by GFAS_FRP. The top part lists results per unit area and the bottom part lists totals.

Site	GFAS_FRP	GFAS_DM	CCI_BA	GFED3_BA	GFED3_DM	GFED4_BA	CCI_BA GFED3_BA	GFED3_DM GFED3_BA
	[kJ m^{-2} a^{-1}]	[g m^{-2} a^{-1}]	[m^2 m^{-2}]	[m^2 m^{-2}]	[g m^{-2} a^{-1}]	[m^2 m^{-2}]	[m^2 m^{-2}]	[kg m^2 a^{-1}]
SS01	27.4	41.7	0.05	0.01	69.5	0.01	*5.82*	*7.9*
SS02	73.7	58.6	0.22	0.05	16.6	0.06	*4.13*	*1.2*
SS03	183.2	167.0	0.15	0.07	63.1	0.07	*2.18*	*3.6*
SS04	36.0	23.2	0.04	0.01	3.4	0.01	*5.11*	*2.0*
SS05	418.9	327.3	0.67	0.22	58.1	0.22	*3.02*	*1.1*
SS06	75.3	57.4	0.18	0.05	8.0	0.05	*3.35*	*0.6*
SS07	36.8	25.3	0.25	0.06	2.1	0.06	*4.26*	*0.2*
SS08	62.4	194.1	0.06	0.01	67.3	0.01	*5.43*	*22.9*
SS09	85.3	132.2	0.04	0.02	16.5	0.02	*1.83*	*4.2*
SS10	169.9	132.5	0.40	0.28	52.0	0.29	*1.40*	*0.7*

Site	GFAS_FRP	GFAS_DM	CCI_BA	GFED3_BA	GFED3_DM	GFED4_BA	CF_GFAS	CF_GFED
	[PJ a^{-1}]	[Tg a^{-1}]	[km^2 a^{-1}]	[km^2 a^{-1}]	[Tg a^{-1}]	[km^2 a^{-1}]	[kg MJ^{-1}]	[kg MJ^{-1}]
SS01	3.8	5.8	7,172	1,232	9.7	1,262	*1.5*	*2.5*
SS02	18.4	14.6	55,214	13,385	16.6	15,474	*0.8*	*0.9*
SS03	45.3	41.2	37,724	17,327	63.1	16,094	*0.9*	*1.4*
SS04	7.0	4.5	8,608	1,686	3.4	1,629	*0.6*	*0.5*
SS05	103.8	81.1	165,963	54,900	58.1	55,308	*0.8*	*0.6*
SS06	19.0	14.5	44,398	13,270	8.0	13,323	*0.8*	*0.4*
SS07	6.1	4.2	41,353	9,701	2.1	10,075	*0.7*	*0.3*
SS08	15.6	48.6	15,949	2,939	67.3	3,434	*3.1*	*4.3*
SS09	14.9	23.0	7,243	3,953	16.5	3,827	*1.5*	*1.1*
SS10	45.6	35.6	106,861	76,071	52.0	76,672	*0.8*	*1.1*

[3] CF for EFOS in GFAS1.0 is 1.55 kg/MJ and CF for PEAT is 5.87 kg/MJ.

Dividing GFED3_DM by GFAS_FRP yields the corresponding CF_GFED in the individual study sites. The CF_GFED/CF_GFAS ratio varies from 0.5 to 1.7. Except for the Russian site (SS09), CF_GFED of these three sites is 40 to 70% higher than CF_GFAS. These high CF_GFED values reflect the spatially and temporally more explicit parameterisation of peat and duff burning in the GFED model. In contrast, the CF values used in GFAS are constant over time and represent average values for the 7 major biomes (see Figure 2.1).

3.2 Correlation across the test sites

Across the test sites, GFAS_FRE (fire radiative energy, which is the time-integrated FRP) and GFAS_DM estimates are highly correlated (zero-forced correlation coefficient R^2 of 0.70; Figure 3.1). The strongest deviation occurs at the test sites SS08 (Russia) and SS09 (Borneo): both sites are linked to elevated PEAT and EFOS conversion factors.

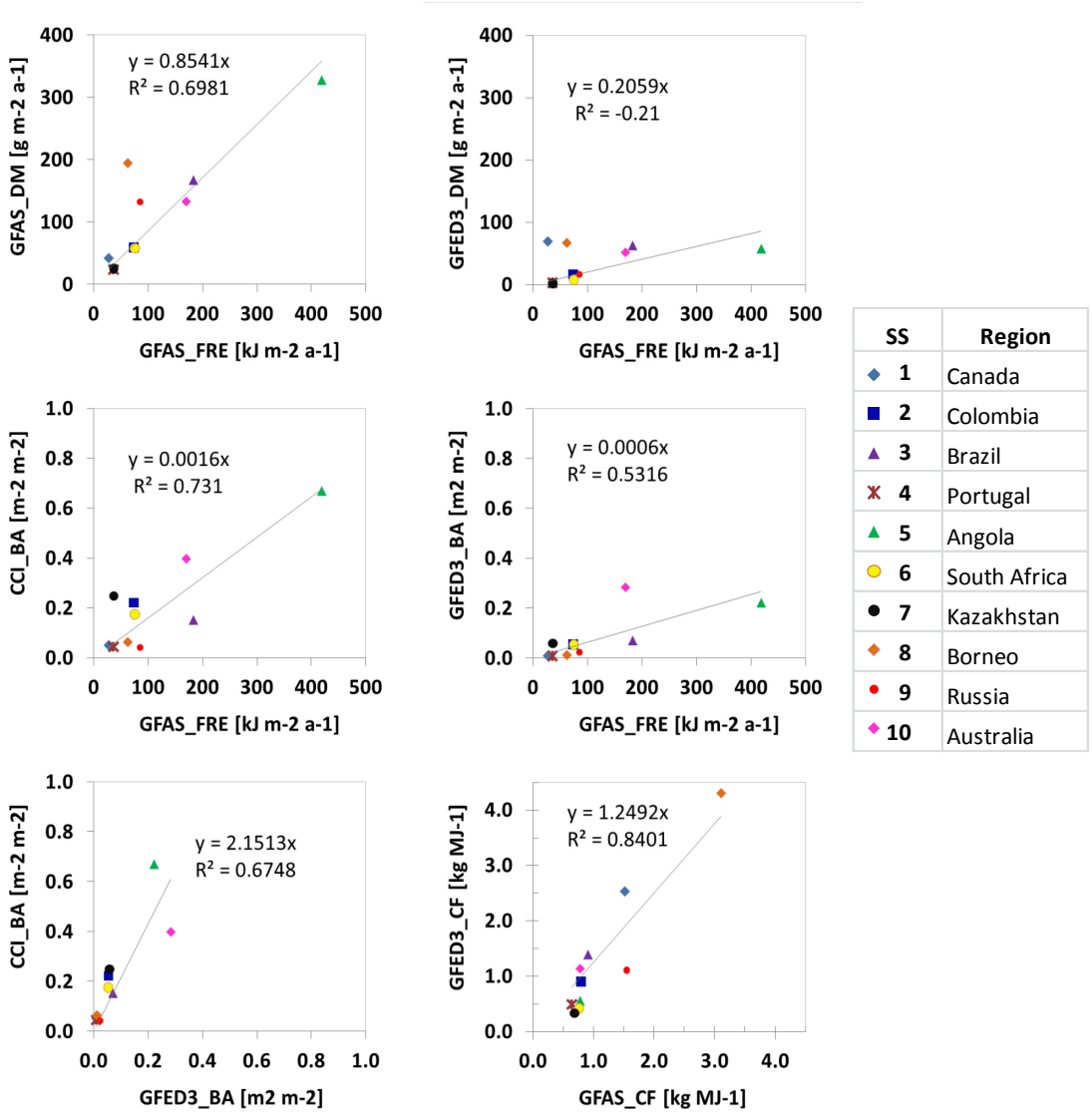

Figure 3.1: Linear correlation of burned area, FRP and dry matter combustion rates between the ten 10 sites.

The site SS05 in Angola has by far the highest mean annual fire radiative energy (FRE) release and, correspondingly, the highest GFAS dry matter combustion rates. SS05 (Angola) is also the test site with by far the highest absolute and relative (related to the domain size) burned area in the CCI_BA product, followed by Australia. In contrast, the test site SS10 (Australia) ranks first in the GFED3_BA product, and SS05 (Angola) only second. The GFAS fraction of observed area in SS05 is close to the average of all other sites. This makes it unlikely that the FRP values are exceptionally biased high, e.g. due to high cloud coverage. Instead, GFED3_BA might underestimate burned area at SS05 since both GFAS_FRP and CCI_BA, are distinctly higher here than at the other sites.

3.3 Number of non-zero grid cells

Table 3.3 lists the total number of grid cells with non-zero values for each month during the period 2003 to 2009 (Ngt0). CCI_BA has the highest number of Ngt0 (Ngt0 = 34,810 summed over all sites). The number of grid cells with fire observations in GFAS_FRP is 7% lower while the number is 43% lower in GFED3_BA and around 48% lower in GFED3_DM and GFED4_BA. A higher Ngt0 value might be related to the capability of CCI_BA and GFAS to detect smaller fires than the MODIS BA product used in GFED. When comparing Ngt0 values as ratio between two products, care has to be taken to avoid numerical artefacts in case of very small values, because the precision at which the data are processed and stored varies among the products. The Ngt0(CCI_BA) / Ngt0(GFAS_FRP) ratio varies strongly across sites. The ratio is highest at test site SS01 (5.5) and lowest for test site SS05 (0.7). Across all sites, Ngt0 for GFED is always lower than in CCI_BA and GFAS_FRP, again highlighting the higher sensitivity of these products in detecting fires.

The linear correlation shows that Ngt0 between different products and parameters is significantly correlated across the sites (Figure 3.2). However, CCI_BA data have a distinct positive offset with respect to GFED and, less pronounced, with respect to GFAS_FRP or GFED_DM. This offset may either indicate the potential of the CCI_BA product to detect relatively small fires, or it could point to commission errors in one of the CCI_BA algorithms[4]. In agreement with these statistics, CCI_BA principally covers a larger spatial extent than GFED as can be seen in Figure 3.3.

Table 3.3: Integrated number of monthly grid cells with values greater than zero

Site	GFAS_FRP	GFAS_DM	CCI_BA	GFED3_BA	GFED3_DM	GFED4_BA
SS01	356	340	1,950	212	139	211
SS02	5,101	5,034	4,515	2,933	2,954	2,113
SS03	4,318	4,251	3,313	2,449	2,337	2,039
SS04	2,223	2,117	2,793	1,022	980	739
S05	5,033	4,979	3,382	3,225	2,802	3,228
SS06	4,732	4,652	4,148	3,200	2,631	3,207
SS07	2,470	2,380	3,646	1,285	1,083	1,333
SS08	2,740	2,685	4,249	1,272	1,263	1,132
SS09	1,367	1,322	1,927	667	554	672
SS10	4,071	3,968	4,886	3,504	3,079	3,500

[4] The merged ESA fire CCI BA product is based on three independent BA retrievals from the three satellite sensors. One would have to look at these individual retrievals in order to identify potential commission errors.

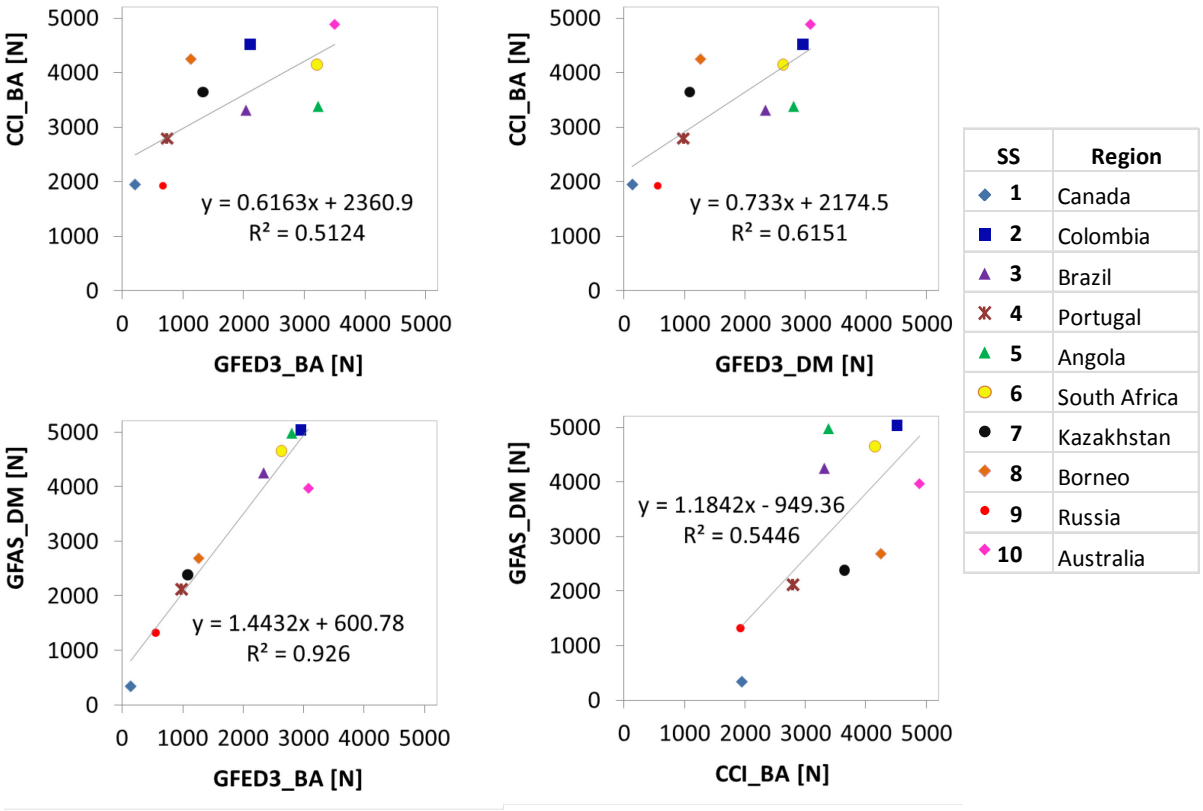

Figure 3.2: Linear correlation of the total number of individual grid cells with non-zero values (monthly burned area, FRP and dry matter combustion rates) between the 10 ESA fire CCI study sites.

During this analysis, we noticed a discrepancy between non-zero GFED3_BA and GFED3_DM grid cells (see Table 3-3 and Figure 3.3). Globally, around 14.5% of Ngt0 (GFED3_BA) have no matching monthly GFED3_DM value. In total, these omitted GFED3_DM grid cells contribute 1.4% to the global area burned, and they are predominantly related to smaller fires (smaller than around 30 km^2 per grid cell and month; see Figure 3.4.

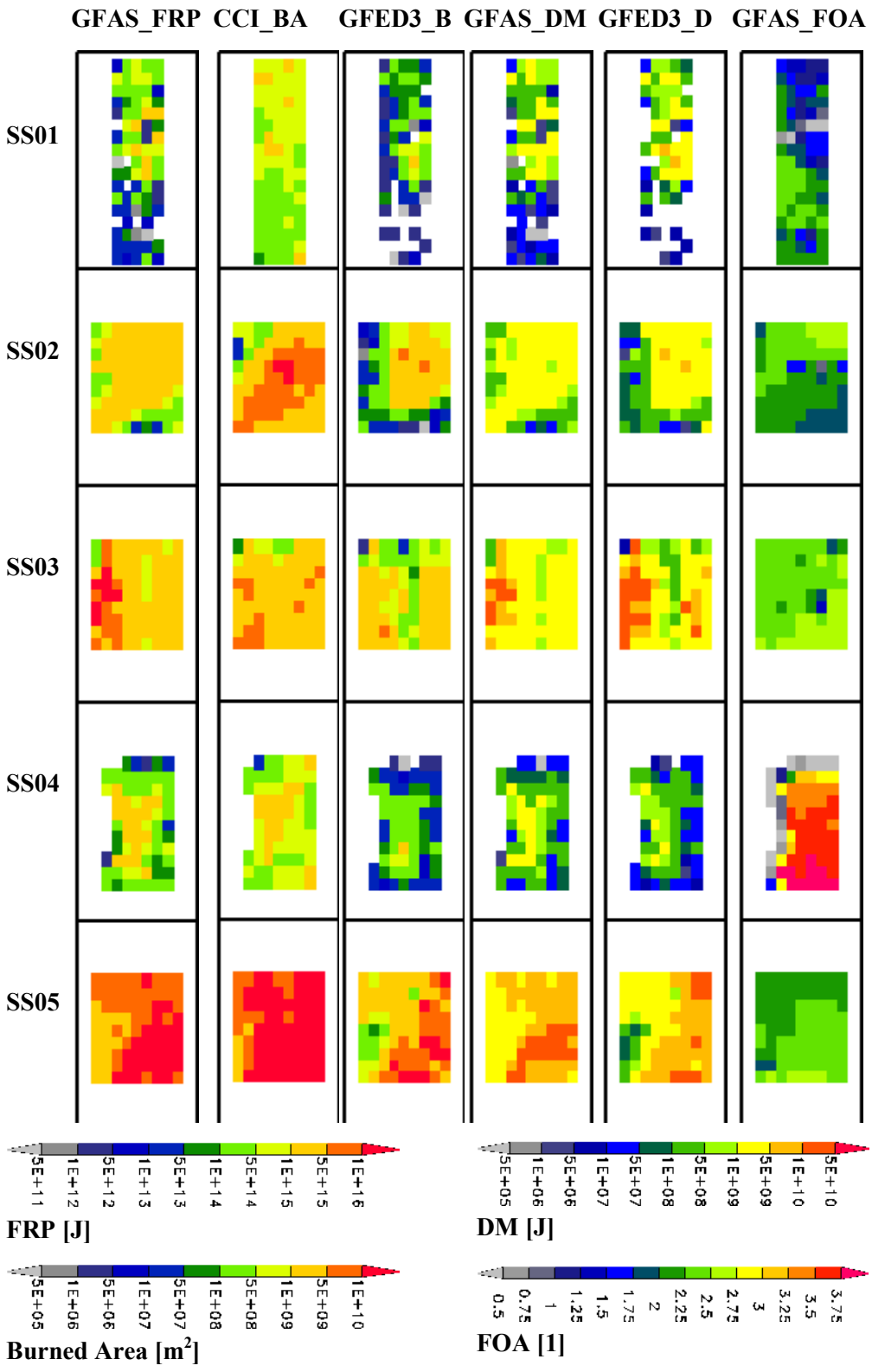

Figure 3.3: Spatial patterns of time-integrated FRP, burned area and dry matter burned estimates over the period 2003 to 2009 for the 10 ESA fire CCI test sites.

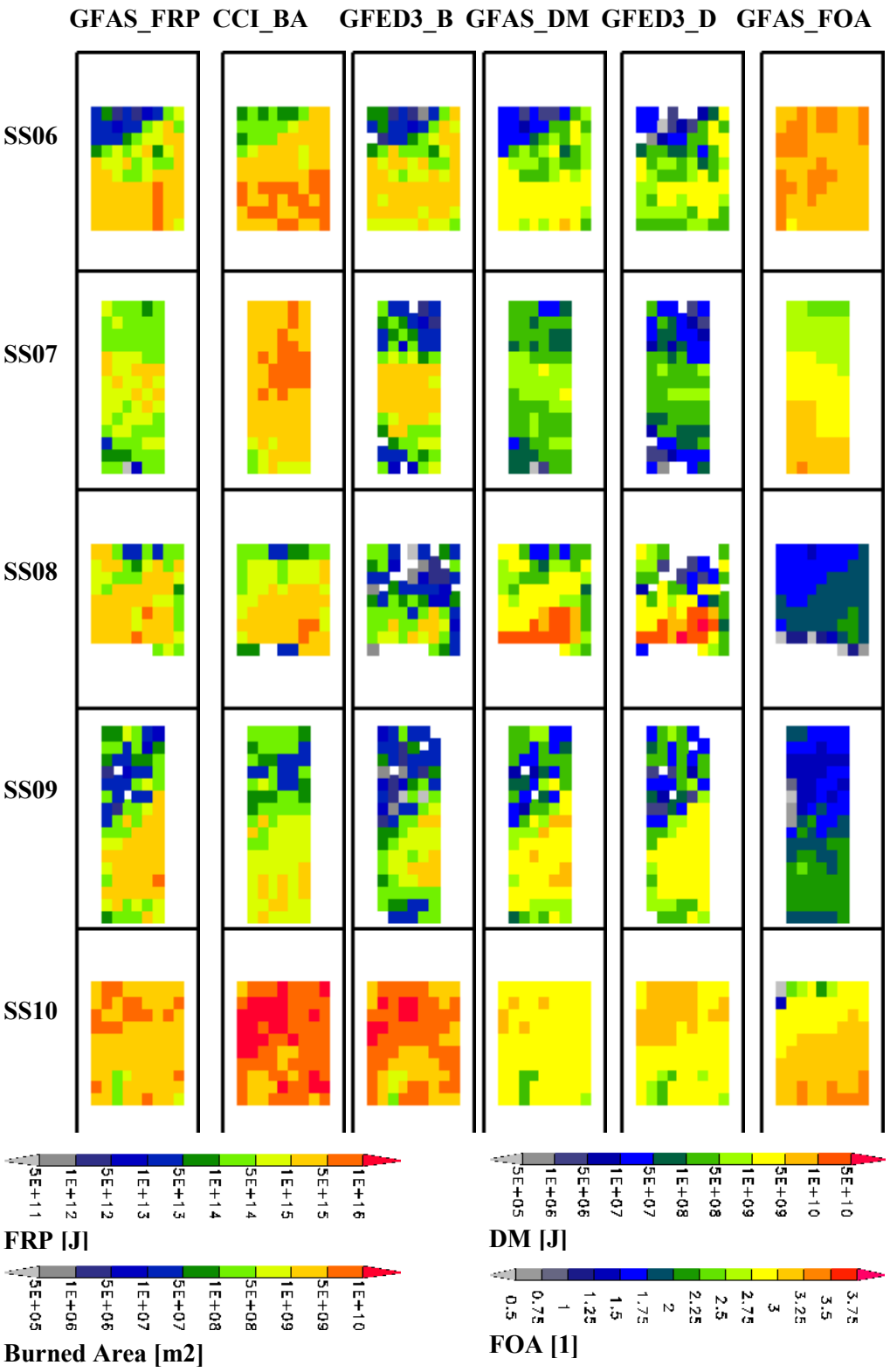

Figure 3.3 continued: Spatial patterns of time-integrated FRP, burned area and dry matter burned estimates over the period 2003 to 2009 for the 10 ESA fire CCI test sites.

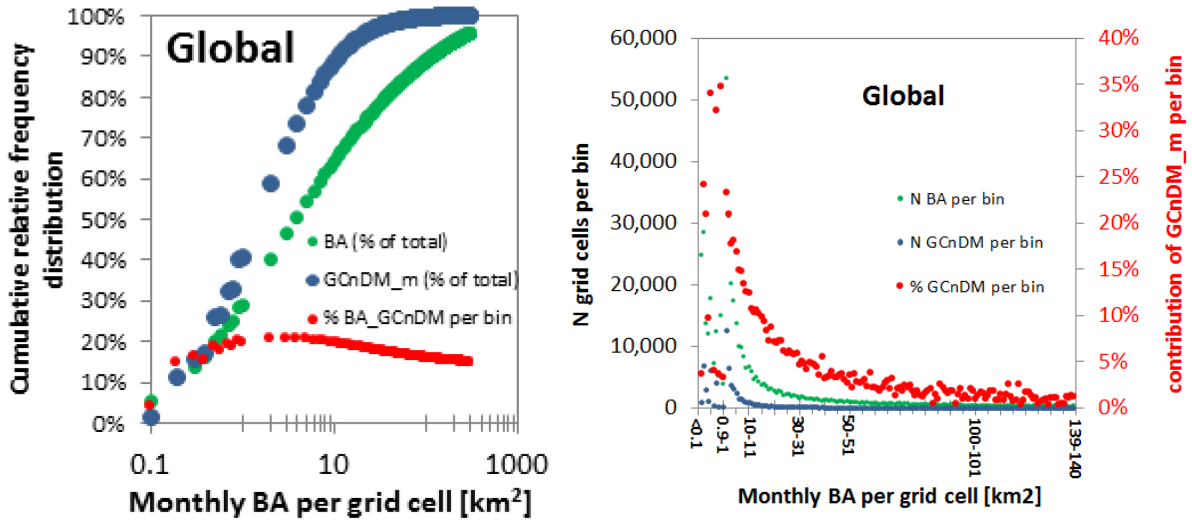

Figure 3.4: Frequency distribution of global monthly burned area in the GFED3_BA dataset and the subset of grid cells with monthly burned area values greater than zero which have no corresponding dry matter burned values greater than zero (GCnDM_m). Bins have 0.1 km² intervals from 0.1 to 1.0 km², and 1 km² intervals for values greater than 1 km².

3.4 Conclusions

The comparison of GFAS and GFED with the preliminary ESA Fire CCI merged burned area product shows that the ESA CCI Fire product yields a much higher total burned area and/or number of grid cells with observed fire activity than the two other inventories, possibly because of its higher sensitivity to small fires. However, commission errors in the ESA fire CCI product cannot be excluded at this stage and should be carefully evaluated. GFAS fire patterns are more similar to ESA CCI BA than GFED, which would confirm the hypothesis of the influence of smaller fires, because GFAS fire detection is based on active fire data with lower detection thresholds than the burned area data used in GFED.

4 Validation Case Studies

In this section we evaluate several case studies where we compare GFAS emission estimates with field measurements and use Chemistry Transport Model (CTM) studies which have been evaluated with atmospheric observations from ground stations, satellites, or aircraft. A quantitative comparison between these studies often remains difficult due to the different transport models, input datasets, and spatial and temporal averaging used in each individual paper, which sometimes leads to contradicting results between studies. Several large fire events in the last years have received considerable attention in the scientific literature (Table 4-1), which gives opportunities to validate bottom-up input datasets for specific regions (Section 4.1). Subsequently, we summarize the literature on larger scale fire emission estimates (section 4.2), and conduct a qualitative comparison of different inversion studies based on either GFED2 or GFED3 biomass burning estimates (Section 4.3). This provides indirect information on the quality of GFAS estimates when results are combined with findings from Section 2. The main findings are summarized in Section 4.4.

4.1 Big fire events

4.1.1 *Russia 2010: Peat and forest fire*

Central Russia suffered from severe forest and peat fires in July and August 2010, and the plumes of these fires severely impacted the Moscow area. Several attempts have been made to estimate total CO emissions from these fires, both using bottom-up and inverse modeling calculations. Huijnen et al. (2011) tested 4 different configurations of the TM5 CTM based on GFED2, GFAS, and two versions with data assimilation of atmospheric CO column retrievals by the satellite-based Infrared Atmospheric Sounding Interferometer (IASI) instrument. The model output was compared with column observations of Measurements of Pollution in the Troposphere (MOPITT) Version 4 (v4) and ground based measurements in the Moscow region. GFAS was found to underestimate emissions somewhat when compared to MOPITTv4, with differences of 22 to 29% for individual hindcast days (Table 4-1). Ground-based observations also indicated that GFAS was too low, with underestimations ranging from 20 to 80%. Similar to CO, an underestimation of GFAS emissions (up to 25%) was found for satellite-based observations of NO_2 from both the Scanning Imaging Absorption spectrometer for Atmospheric CHartographY (SCIAMACHY) and the Ozone Monitoring Instrument (OMI).

Konovalov et al. (2011) used surface CO measurements in Moscow collected during the fire episode to scale aboveground and peat burning emissions in the regional CHIMERE CTM. When they applied a strong diurnal cycle total emissions of 10 Tg CO were derived for central European Russia in July and August 2010, while GFAS estimates 13.31 Tg CO for the corresponding time and period (Table 4-1). Krol et al. (2013) estimated CO emissions by combining TM5-4DVAR and column measurements from IASI. From mid-July to mid-August 2010 their emission estimate was on average 24 Tg CO, which is less than other inverse modeling studies (Yurganov et al., 2012; Fokeeva et al., 2012), but significantly higher than all bottom-up emission inventories including GFAS.

Globally, GFAS was found to underestimate aerosol optical depth (AOD) by a factor of 3.4 (Kaiser et al., 2012). Applying this correction factor over the region of the western Russian fires the GFAS aerosol emissions are consistent with eastern European AERONET observations (Kaiser et al., 2012). Additionally, Huijnen et al. (2011) used the scaled GFAS aerosol emissions in a CTM simulation and compared modeled AOD to the measurements from an AERONET station at Moscow. The agreement varied as a function of hindcast day, with model results ranging from 28% below to 12% above the in situ reference observations.

4.1.2 *Greece 2007: Forest and shrubland fires*

The Greek fires in August 2007 were studied by several authors to estimate the total amount of trace gases emitted. Turquety et al. (2009) estimate an emission of the 336×10^3 tons of CO from IASI plume observationsfor 23-30 August. Their error analysis leads to the conclusion “that the value inferred here should be on the low end of the actual CO emissions”. They also perform a burnt area-based calculation of the CO emissions and reach a value of 348×10^3 tons. The CO emissions in GFAS from the Peloponnesus during 23-30 August were 417×10^3 tons. Thus they appear to be high estimates by 20-24% in this case. GFED3 estimates a much lower value of 71×10^3 tons for the corresponding time and area.

Coheur et al. (2009) also use retrievals from IASI, and find elevated concentrations of CO in the smoke plumes, reaching 2.74×10^{19} molecules cm^{-2}. However, they don't derive an emission budget for CO. Based on retrievals of NH_3, C_2H_4 and CH_3OH on 25 August 2007, Coheur et al. (2009) estimate emissions of 40×10^3, 6.5×10^3 and 7.0×10^3 tons for these species, respectively from the Peloponnese fires. The authors call these number "only indicative" due to large, not further quantified uncertainties. The emissions from GFAS for this date and area were 2.4×10^3, 2.8×10^3, and 4.8×10^3 tons, corresponding to a potentially large underestimation (Table 4-1).

4.1.3 *Alaska and Canada 2004: Forest fires*

The forest fires in Alaska and Canada that burned from mid-June until September 2004 were among the largest on record for the boreal regions. To quantify the emissions of these fires, Pfister et al. (2005) used CO data from the MOPITT instrument together with the MOZART CTM. Their inverse modeling resulted in a total of 30±5 Tg CO emitted during June – August 2004, which is 27±21% higher than the GFAS estimate (Table 4-1).

Turquety et al. (2007) constructed a daily bottom-up fire emission inventory for the 2004 fire season in North America, including consideration of peat burning and high altitude injection. Their total estimate of the fire emissions during the summer of 2004 was also 30 Tg CO, including 11 Tg from peat. They found that including peat burning in the GEOS-Chem simulation improves agreement with MOPITT observations. Bottom-up GFAS estimates give a total of 23 Tg CO for this period, corresponding to a difference in emissions of 22% (Table 4-1).

Elguindi et al. (2010) studied the long-range transport of biomass burning emissions from the 2004 boreal fires in Alaska and Canada, based on the MACC reanalysis (Inness et al., 2013) and a reference simulation without data assimilation, which were compared to data from the Measurement of Ozone and Water Vapour on Airbus In-service Aircraft (MOZAIC) aircraft program. The MACC reanalysis, which applied fire emissions based on a preliminary version of GFED3.0 (v3.0), performed better than the standalone CTM, but the modeled plumes were still too weak and occurred at the wrong altitude. With the emission inventory of Turquety et al. (2009) the model results improved.

4.1.4 *Alaska 2007: Tundra fire*

Mack et al. (2011) conducted an in-situ study of the burnt area and burn depth of the Anaktuvuk River fire in 2007 that burned 1039 km^2 of Alaska's arctic slope, making it the largest fire on record for the tundra biome. The study reports that the tundra ecosystem lost ~2.1±0.4 Tg C overall in the fire. This compares reasonably well to the total carbon consumption of 1.7 Tg C included in GFAS (Table 4-1). This reasonably good agreement with GFAS, despite GFAS not including tundra as a separate biome, underlines the robustness of the FRP-based approach.

4.1.5 *Siberia 2003: Wildfires*

The carbon release of the southern Siberia 2003 wildfires (close to Lake Baikal) was analysed by Huang et al. (2009) using Advanced Very High Resolution Radiometer (AVHRR), MODIS, Medium Resolution Imaging Spectrometer (MERIS), and Advanced Spaceborne Thermal Emission and Reflection Radiometer (ASTER) images and a carbon release model. Three levels of fire severity under different scenarios were represented, and they computed carbon emissions between 401 Tg and

684 Tg C for the year 2003. GFAS bottom-up estimates of 218 Tg C were respectively 46 and 68% lower compared to the standard and extreme scenario, and this underestimation might be due to the poor representation of peat areas within the bottom-up modeling framework.

4.1.6 *Australia 2009: Black Saturday fires*

In February 2009, the "Black Saturday fires" took place in the South East of Australia, and large quantities of aerosol and pollutants were emitted into the atmosphere. Satellite observations by the Global Ozone Monitoring Experiment (GOME)-2 instruments show a large plume of NO_2, HCHO, and CHOCHO extending from Australia all the way to the southern tip of New Zealand. The MACC reanalysis nicely reproduced the shape of the plume leaving Australia on February 7, 2009 and simulated correctly that only weak plumes remained on February 8, in agreement with satellite data (Melas et al., 2013). The absolute NO_2 values within the plume were in good agreement between model and measurements. The satellite data are slightly larger but, given the uncertainties due to cloud cover, the agreement is good (Melas et al., 2013).

4.2 Distributed fire activity

In addition to validation of GFAS estimates for specific fire events, we discuss in this section various regional and global studies of biomass burning emissions for several species.

4.2.1 *CO*

An extensive validation report of the MACC reanalysis (which employed fire emissions based on GFED3.0, MODIS FRP for 2003-2008 and GFASv1.0 for 2009-2010) focused on several biomass burning regions and species (Melas et al., 2013). Figure 4.1 shows that the MACC reanalysis captures the seasonal and inter annual variability of CO total columns as observed by MOPITT and IASI well for fire regions in Alaska, Siberia, and Africa. In the boreal regions a negative difference (up to 19%) between the reanalysis and MOPITT and IASI was found during the biomass-burning season. In northern Africa the MACC reanalysis showed positive differences up to +18% compared to MOPITT in the peak fire months, but this bias decreased after 2004 (Figure 4.2). In southern Africa the difference compared to both MOPITT and IASI was overall positive (0 – 10%) in the burning season.

Vertical profiles of biomass burning plumes of CO at Windhoek, Namibia, as sampled by MOZAIC observations, were captured within 10%. This illustrates that the applied fire emissions were appropriate (Melas et al., 2013). These findings were also confirmed by the NO_2 evaluation over southern Africa.

Table 4.1: Overview of validation case studies. The colours correspond to the different fire events that were used in the validation attempts.

Location & year	Reference	Species	Emission estimate[1]	GFASv1.0 estimate	Difference[2] (%)
Russia 20 July – 15 August, 2010	Huijnen et al. (2011)[3]	CO	15.64 Tg 17.18 Tg	12.2 Tg	-22% -29%
Russia 20 July – 15 August, 2010	Huijnen et al. (2011)[4]	CO	15.25 Tg 61 Tg	12.2 Tg	-20% -80%
Russia 20 July – 15 August, 2010	Huijnen et al. (2011)[3]	NO_2	79 Gg 85 Gg	71 Gg	-10% -15%
Russia 20 July – 15 August, 2010	Huijnen et al. (2011)[4]	NO_2	91 Gg 95 Gg	71 Gg	-22% -25%
Russia 20 July – 15 August, 2010	Huijnen et al. (2011)	AOD	x	x	-28% +12%
Russia June – August, 2010	Krol et al, (2013)	CO	22 Tg 27 Tg	13.31 Tg	-39% -51%
Russia June – August, 2010	Konovalov et al. (2011)	CO	10 Tg	13.31 Tg	+33%
Russia June – August, 2010	Yurganov et al. (2011)	CO	34 Tg 40 Tg	13.31 Tg	-61% -67%
Russia June – August, 2010	Fokeeva et al. (2010)	CO	29.8 Tg 36.1 Tg	13.31 Tg	-55% -63%
Russia June – August, 2010	Fokeeva et al. (2010)	CH_4	1.6 Tg 1.9 Tg	1.21 Tg	-24%
Russia June – August, 2010	Kaiser et al. (2012)	AOD	x	x	-71% (Factor 3.4)
Greece 25 August, 2007	Coheur et al. (2009)	NH_3	40 Gg	2.4 Gg	-94%
Greece 25 August, 2007	Coheur et al. (2009)	C_2H_4	6.5 Gg	2.8 Gg	-57%
Greece 25 August, 2007	Coheur et al. (2009)	CH_3OH	7 Gg	4.8 Gg	-31%
Greece 23-30 August, 2007	Turquety et al. (2009)	CO	336 Gg 348 Gg	417 Gg	+24% +20%
Alaska and Canada June – August, 2004	Pfister et al. (2005)	CO	30±5 Tg	23.44 Tg	-22%
Alaska and Canada June – August, 2004	Turquety et al. (2007)	CO	30 Tg	23.44 Tg	-22 %
Alaska 2007	Mack et al. (2011)	C	2.1±0.4 Tg	1.7 Tg	-19%
Siberia 2003	Huang et al. (2009)	C	401 Tg 684 Tg	217.75 Tg	-46% -68%

[1] *Emission estimates from validation studies. Two emission estimates for one specific case study correspond to different model assumptions or hindcast days.*

[2] *Difference (%) in emission estimates between GFAS and validation study estimates, as a percent of validation study estimates: Positive numbers indicate that GFAS is higher than study estimates and vice versa.*

[3] *Satellite-based comparison*

[4] *Ground-based comparison*

4.2.2 *NO_2*

The study of Inness et al. (2013) compares the MACC reanalysis with SCIAMACHY retrievals of the tropospheric NO_2 column for several biomass burning regions in the years 2003 to 2010. NO_2 fields from the reanalysis show the right seasonality over tropical biomass burning areas, but in northern and southern Africa NO_2 is overestimated during the tropical biomass burning seasons (average difference of 53%; Figure 4.3). For northern Africa similar results were found by Melas et al. (2013), who also performed a comparison between model columns of tropospheric NO_2 to values retrieved from SCIAMACHY satellite observations. However, in the southern part of Africa the agreement between MACC reanalysis NO_2 and SCIAMACHY data was very good with the model being only slightly higher (~10%) during the fire season (Figure 4.4). There was no good explanation for these differences found for northern and southern Africa (Melas et al. 2013).

4.2.3 *HCHO (Formaldehyde)*

Inness et al. (2013) also performed a comparison between the MACC reanalysis and SCIAMACHY observations of HCHO for the African continent in the years 2003-2010. Overall the simulated HCHO showed a good agreement with the SCIAMACHY retrievals over the African continent (Figure 4.5): in northern Africa the MACC reanalysis overestimated satellite observations (maximum of ~20%) during the biomass burning months, while in southern Africa an underestimation was found of ~15%.

4.2.4 *AOD*

Huneeus et al. (2012) performed emission estimates of a range of aerosol species at the global scale and used MODIS AOD and AERONET measurements and a global aerosol model for comparison. At the stations of Mongu (South Africa; 15.25º S, 23.15º E), Abracos Hill (South America; 10.76º S, 62.36º W) and Jabiru (Australia; 12.66º S, 132.89º E), all influenced by biomass burning emissions, the first guess a-priori underestimates the AOD throughout the year by roughly a factor of 3, similar to the findings of Kaiser et al. (2012). Discrepancies between top-down and bottom-up estimates of smoke aerosol emissions are generally found in the scientific literature, and the top-down estimates are generally larger by factors in the range of 1.5 to 4.

4.2.5 *POP*

As an extension to GFASv1.0, a vegetation fire emission inventory of persistent organic pollutants (POPs), polychlorinated dibenzo-p-dioxins (PCDDs) and -furanes and polycyclic aromatic hydrocarbons (PAHs), has been created based on a detailed emission factor review. POPs have various acute and chronic effects on humans, with some of them being carcinogenic. The GFAS POP inventory was used as input for global multi-compartment chemistry transport model simulations (Lammel et al., 2013). The aim of the model study was to validate modeled atmospheric POP concentrations against station measurements in Africa and to assess the relative contribution of biomass burning POPs to the regional POP burdens.

In contrast to other compounds, there are no POP emission factors from field measurements of grassland or forest fires. As a proxy, emission factors measured in open burning simulation facilities were used, which are associated with large uncertainty. The PAH emission factors for a given fuel category (wood or agriculture/grassland), for example, vary by 2 orders of magnitude. For the model study, a best guess estimate calculated from the geometric mean was used. Due to the multiphase

nature, POP emissions are distributed in the atmosphere, the hydrosphere and the pedo- and biosphere, and are therefore very complex to parameterise in models, adding to the overall uncertainty of this model study.

The comparison with field measurements at rural background sites in Africa indicated that model predicted vegetation fire emissions explain up to 100% of PAH levels. Benz(a)pyrene (BAP) levels are typically over predicted, possibly due to overestimated emission factors and/or underestimation of atmospheric sinks. Model predicted vegetation fire emissions typically explain 1 to 10% of the observed dioxin and furan levels. The model results also support a regional long-range transport potential of dioxins and furans, and also of PAHs as suggested in earlier studies (e.g. Friedman and Selin, 2012).

This is the first multi-compartment modeling study so far which analyses the contribution of POP emissions from vegetation fires on ambient POP levels using a spatially and temporally explicit vegetation fire emission inventory (GFAS POP emission inventory). Despite various uncertainties in the emission estimates and the modeled atmospheric processes, this study suggests that vegetation fires contribute significantly to the exposure of the African environment to PAH and dioxins. This is an example of GFAS being extended and used in a scientific application. The feedback on the accuracy of GFAS is limited to the qualitative finding that the emissions are reasonable and their order of magnitude is correct.

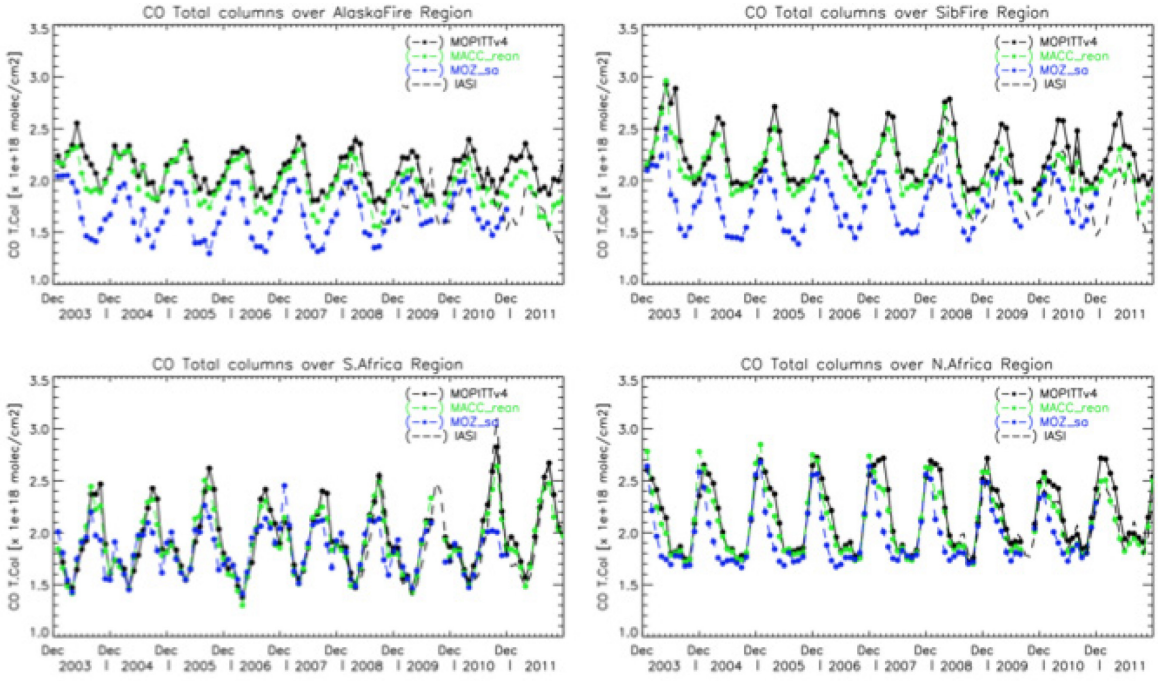

Figure 4.1: Regionally averaged CO total columns simulated by the MACC reanalysis and the corresponding MOZART stand alone run for the 2003-2011 period compared with MOPITTv4 and IASI observations over 4 selected regions. ***From Melas et al. (2013)***

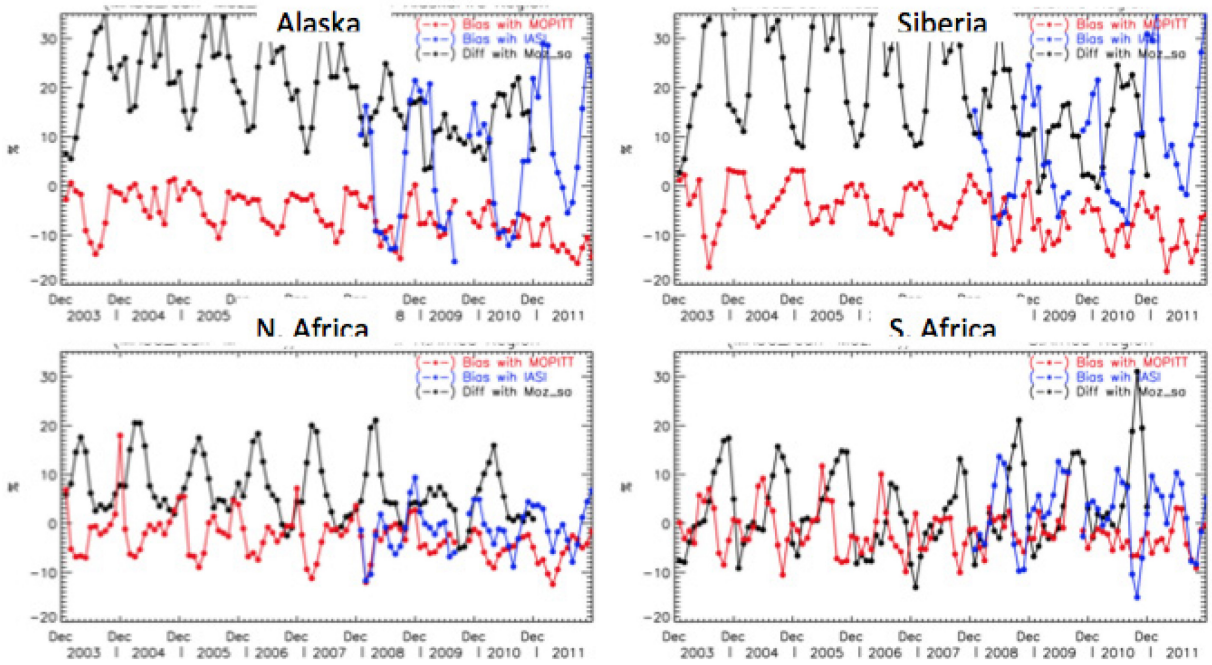

Figure 4.2: Relative differences between MACC reanalysis CO total columns and MOPITT, IASI observations and MOZART stand-alone results over 4 selected regions during the 2003-2011 period. ***From Melas et al. (2013)***

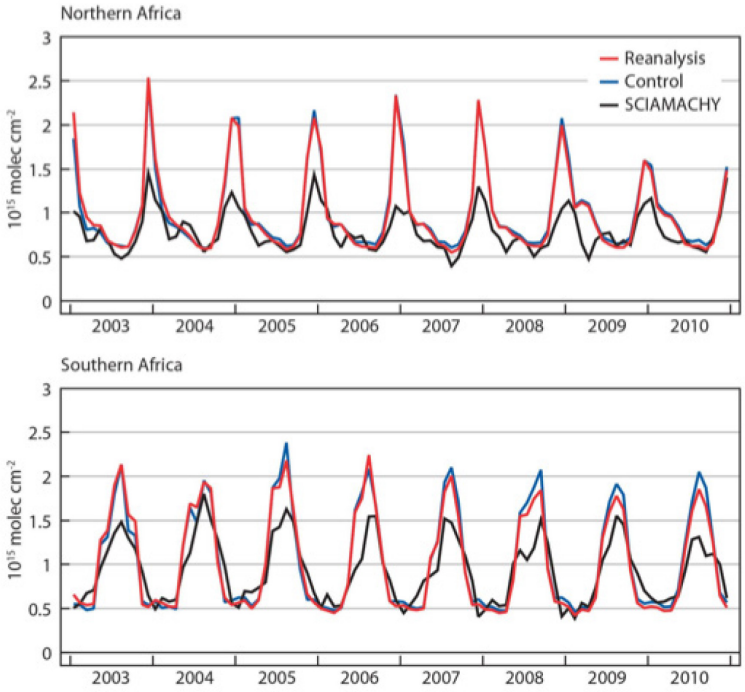

Figure 4.3: Time series of monthly mean area averaged tropospheric NO2 columns in 10^{15} molecules cm^{-2} from the MACC reanalysis (red), the control run (blue) and from IUP-SCIAMACHY data (black) for the period 2003 to 2010 for Northern Africa (top) and Southern Africa (bottom). ***From Inness et al. (2013)***

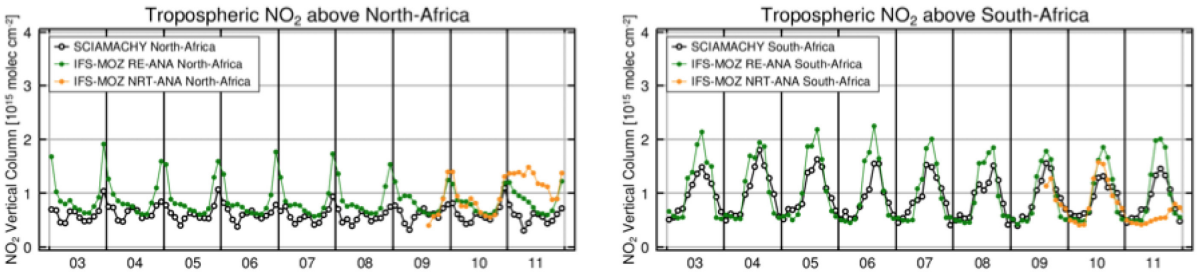

Figure 4.4: Comparison of time series of tropospheric NO_2 columns from SCIAMACHY and model results over northern and southern Africa. ***From Melas et al. (2013)***

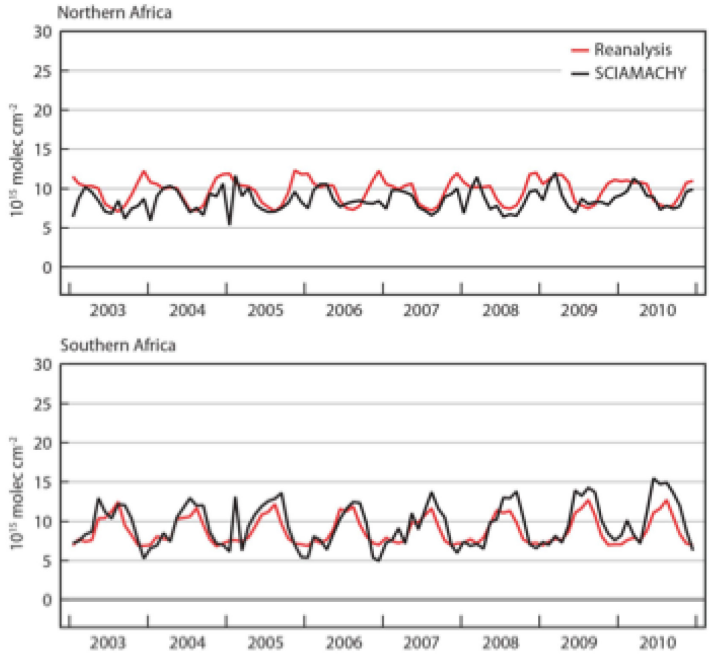

Figure 4.5: Time series of monthly mean area averaged tropospheric HCHO columns in 10^{15} molecules cm^{-2} from the MACC reanalysis (red), the control run (blue) and from IUP-SCIAMACHY data (black) for the period 2003 to 2010 for Northern Africa (top) and Southern Africa (bottom). ***From Inness et al. (2013)***

4.3 Qualitative comparison with inverse modeling studies

To complement the studies from section 4.2 that directly used GFAS emissions, we evaluated inversion studies that often used atmospheric measurements in combination with satellite derived CO columns to constrain GFED emissions for several important fire regions (Table 4-2). Since the focus of these studies is on bottom-up emission estimates from GFED2 or GFED3, we used the findings shown in Section 2 to convert GFED-based results to an estimate for GFASv1.0. Clearly, a quantitative comparison between studies remains difficult due to the different transport models, input datasets, and spatial and temporal averaging used in each individual paper. Therefore this section is based on qualitative analysis, and only shows the general trends for different regions. An overview of

the regions defined in Table 4.2: Qualitative comparison of different inversion studies based on either GFED2 or GFED3 biomass-burning estimates. The '+' and '-' signs indicate that respectively higher and lower CO concentrations were estimated for GFASv1.0 compared to the inversion study. The '=' sign indicates that results were in close agreement with GFASv1.0 (within ~5%). is shown in Figure 2.1. In general the GFASv1.0 converted emission estimates are too low in the boreal regions (BONA and BOAS), Equatorial Asia (EQAS), and Africa (SHAF and NHAF) compared to most of the inversion studies. In Australia (AUST) and South America (SHSA) the results are more mixed. The results for GFED3 estimates compare very well to results shown here (*van Leeuwen et al.,* 2013). These results are overall consistent with the findings of Section 4.1 and Table 4-1 and thus support the finding of a general slight underestimation of the CO emissions with large regional variations.

Table 4.2: Qualitative comparison of different inversion studies based on either GFED2 or GFED3 biomass-burning estimates. The '+' and '-' signs indicate that respectively higher and lower CO concentrations were estimated for GFASv1.0 compared to the inversion study. The '=' sign indicates that results were in close agreement with GFASv1.0 (within ~5%).

Study / Region	Year	BONA	BOAS	SHSA	SHAF	NHAF	EQAS	AUST
Hooghiemstra et al., 2011	**2004**	-		-	-	-		+
Kopacz et al., 2010	**2004**	-	=	=	-	-	-	-
Pison et al., 2009	**2004**	=	-	=	-	-	-	+
Jones et al., 2009	**2004**	=		-	-	-		-
Chevallier et al., 2009	**2004**				-	-		
Gonzi et al., 2011	**2006**	-	-	+			-	
Hooghiemstra et al., 2012	**2006 - 2010**			-				
Fortems-Cheiney et al., 2011	**2005-2010**	-		-			+	-

4.4 Discussion / conclusions

Compared to most published investigations, GFAS appears to reflect the "state-of-the-art" in emission estimation. Uncertainties appear to be typically around 30%, and larger for exotic species. A tendency to underestimate appears in several fine-scale detailed investigations, but overestimation is also being reported in several cases. Aerosol emissions require dedicated attention, therefore Kaiser et al. (2012) introduced a factor 3.4 to match GFAS emissions with observations of AOD, corresponding to a difference of roughly 70%. However, this large amplification is more likely to be related to issues in the modeling of aerosols, in particular to rapid evolution/ageing of smoke aerosols in the high concentration environment of the initial smoke stack and plume, than the result of errors in the emission estimates, per se.

A qualitative comparison with inverse modeling studies based on CO showed consistent results for the boreal regions, with GFAS emissions being too low in both boreal North America (BONA) and Asia (BOAS). Krol et al. (2013) argue that most bottom-up emission estimates in the boreal regions are biased low, and have to be enhanced to match satellite observations. A reason for these underestimations may be the poor representation of peat areas within the bottom-up modeling framework. However, for a boreal Tundra fire the GFAS performance was excellent and the good agreement underlines the robustness of the FRP-based approach.

Over the African continent we found that GFAS emissions were generally in good agreement (within ~20%) with several validation studies. GFAS estimates of HCHO were slightly too low compared to satellite-based column measurements. NO_2 emissions, on the other hand, were often estimated too high for both northern and southern Africa, and similar results were found for CO. Several inverse modeling studies showed a different pattern, with most of the studies estimating higher CO values compared to GFAS. For Equatorial Asia (EQAS), Australia (AUST) and South America (SHSA), the inverse modeling results were more mixed, with no clear under- or overestimation of GFAS for the different studies. However, one should be careful to draw conclusions with respect to the quality of GFAS based on these studies, because they yield conflicting results due to the use of different models and observations.

A validation case study of the 2007 fires in Greece showed that GFAS overestimated satellite-based observations of CO by 24% but underestimated C_2H_4, CH_3OH, and NH_3 significantly, with differences up to 94% for NH_3. However, the satellite-based CO estimate is likely to be biased low itself and uncertainties for all satellite-based estimates are large but not quantified. Unfortunately this is the only validation study we are aware of, and given the fact the underestimation of GFAS was rather large, these less-frequently measured species should deserve more attention in future validation attempts.

5 GFAS design features

This section discusses key aspects of the GFAS algorithm and implementation that have been flagged during the ongoing development. We start discussing characteristics of the MODIS instruments and FRP observations (Section 5.1 until 5.4), then we discuss the calculation of emissions from the FRP observations (Section 5.5 and 5.6), and finally some issues related to general model development (Section 5.7 and 5.8) and its operational status (Section 5.9). Conclusions are provided in section 5.10.

5.1 MODIS observations near the swath edge

The MODIS instruments on the Aqua and Terra satellites achieve a global coverage of around 4 scans a day by using a wide swath (with viewing geometry being ±65º on each side of nadir). The drawback of this method is that sensors have a higher detection threshold towards the swath edge, resulting in a lack of observations of small fires. In general, regions closer to the sub-satellite track will show higher FRP (and therefore emissions) than regions that are covered near the swath edges. The EOS satellites are polar orbiting and have therefore more overpasses close to the poles and less around the equator. As a result the emission estimates exhibit an oscillation with an interval of around two days near the tropics (i.e., one day will be captured well and the next one will be underestimated). The FRP used in

GFAS is an average of the daily observations (Kaiser et al., 2012). The 'oscillation' is expected to be more pronounced in the tropics than in the polar regions, close to the poles, there is significant overlap between MODIS images resulting in more than four daily observations.

Days with higher FRP are more realistic than those with lower FRP. Therefore, the average FRP of GFAS is an underestimation. However, the average dry matter combustion and emission rates include a compensation for the FRP underestimation because the conversion factors have been derived consistently for the monthly average dry matter combustion rates of GFED and the monthly average FRP as represented in GFAS. Assuming GFED emissions to be correct, daily GFAS emission estimates are alternatingly over- and underestimated.

Figure 5.1 shows a comparison between estimated GFAS Fire Radiative Energy (FRE; i.e., integrated FRP) and the estimated 'oscillation free' FRE, ignoring the days of no direct overpasses for a tropical savanna in northern Africa and a boreal forest in North America. For the study region in northern Africa, GFAS FRE estimates were 22.4 PJ over the study period (burning season of 2003-2004), while the oscillation free estimates were 29.8 PJ, thus implying an underestimation by ~25% (Figure 5.1a). Figure 5.1b shows a similar figure but for North American fires in 2004. Although the relative difference between the observed FRE (38.4 PJ) and the 'oscillation free' FRE (49.8 PJ) for North

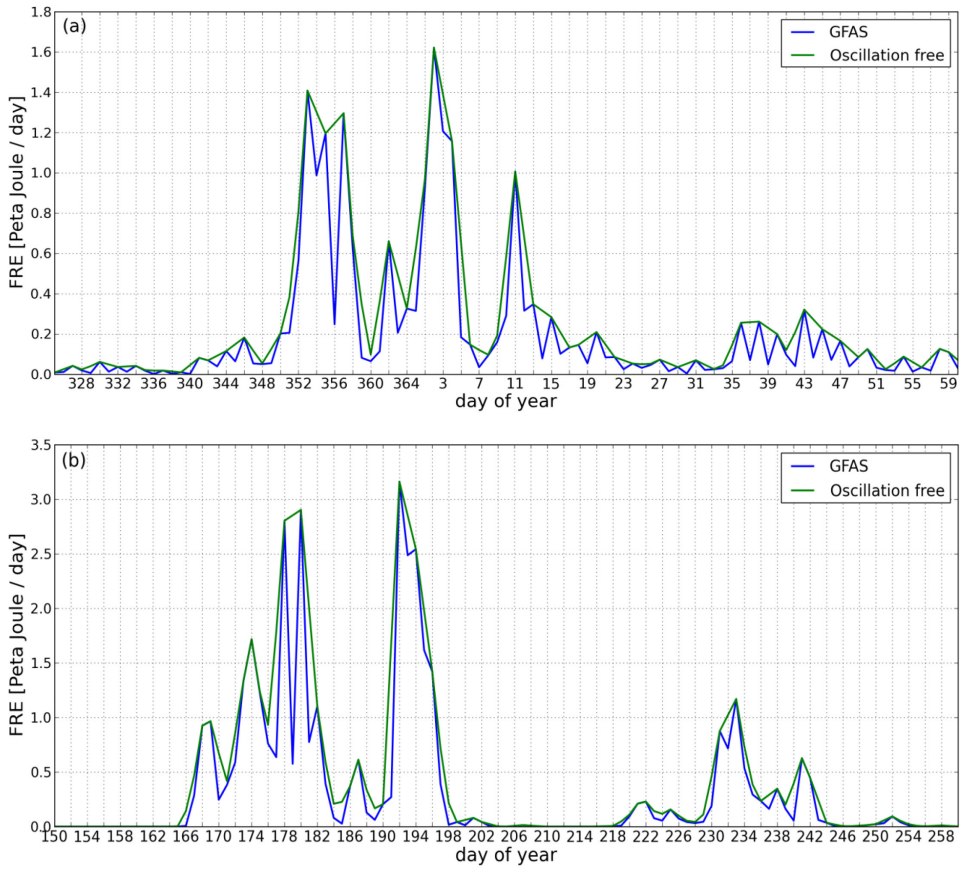

Figure 5.1: GFAS observed Fire Radiative Energy (FRE) and estimated oscillation free FRE, if days without direct overpasses are ignore for two selected 2° regions. Panel (a) shows the 2003-2004 burning season for a selected region in northern Africa (4.5-6.5°N 31-33°E); and panel (b) the selected region in North America (65.5-67.5°N 147-145°W) for the summer of 2004.

American boreal fires are similar to those of northern Africa (25% and 23% too low, respectively), the 2-day oscillation pattern is less pronounced. This is likely due to the fact that more daily observations were available over which the mean is calculated. Although the GFAS conversion factors from FRP to DMb compensate for the observed effect and mean emission estimates over a given period of time are realistic, daily GFAS emission estimates might be too high or too low.

5.2 Diurnal cycle

The intensity of burning is commonly characterized by a typical diurnal cycle depending on vegetation type, region, and meteorological properties (Giglio, 2007). MODIS observations are made at fixed moments in time for the Terra (10:30 h and 22:30 h local time) and Aqua (13:30 h and 01:30 h) satellites, respectively. GFAS assumes observations to be valid until the next observation (Kaiser et al., 2012). In GFAS, structural deviations are partially accounted for by conversion factors. Yet, with only two overpasses during daytime one has to make assumptions regarding the diurnal evolution of fires, which are not always correct.

With geostationary satellites, it is possible to characterize the diurnal cycle of fire activity. Considerable efforts have been made already to integrate fire retrievals from geostationary satellites into GFAS, but until now it was impossible for MACC-II and other groups to achieve consistency with the MODIS FRP data set due to large variability of the bias between the two types of observations. The detection threshold of geostationary satellites is larger by up to an order of magnitude than the one of MODIS. Therefore SEVIRI misses so many small fires that it records on average about half of the FRP per grid cell compared to MODIS. However, the percentage depends on the actual fire size distribution and thus varies with land cover type, fire season, fire weather and local time. A short-term improvement of GFAS could be made by integrating “typical diurnal cycles” from the geostationary observations. This might considerably improve the estimation of fire activity, especially if only a limited number of observations are present, for example due to cloud cover. However, one needs to carefully define the regions for which this is possible.

Melas et al. (2013) compare SCIAMACHY observations of NO_2 and HCHO, observed in the plumes from the Australia Black Saturday fires in 2009, to the MACC reanalysis. They find that the “shape of the plume is well captured” but that the maximum values within the plumes are shifted within the plumes. This may be attributed to temporal patterns in the emissions not being properly described. A change of the temporal resolution of GFAS from 24 hours to 1 hour would allow for a more accurate temporal description of the emissions.

5.3 Quality control of input data

A few of the MOD14/MYD14 MODIS active fire data sets contain individual pixels with extremely large values, which are obviously unrealistic but can even dominate the corresponding global monthly emission budget if they enter the analysis. An example is shown in Figure 5.4. GFAS checks two threshold values to detect such unrealistic outliers and subsequently removes all observations of that day from further processing. As a consequence, GFAS falls back to assuming persistency of fire activity from the previous day. This is illustrated in Figure 5.5 for 30 July 2010. Neglecting more

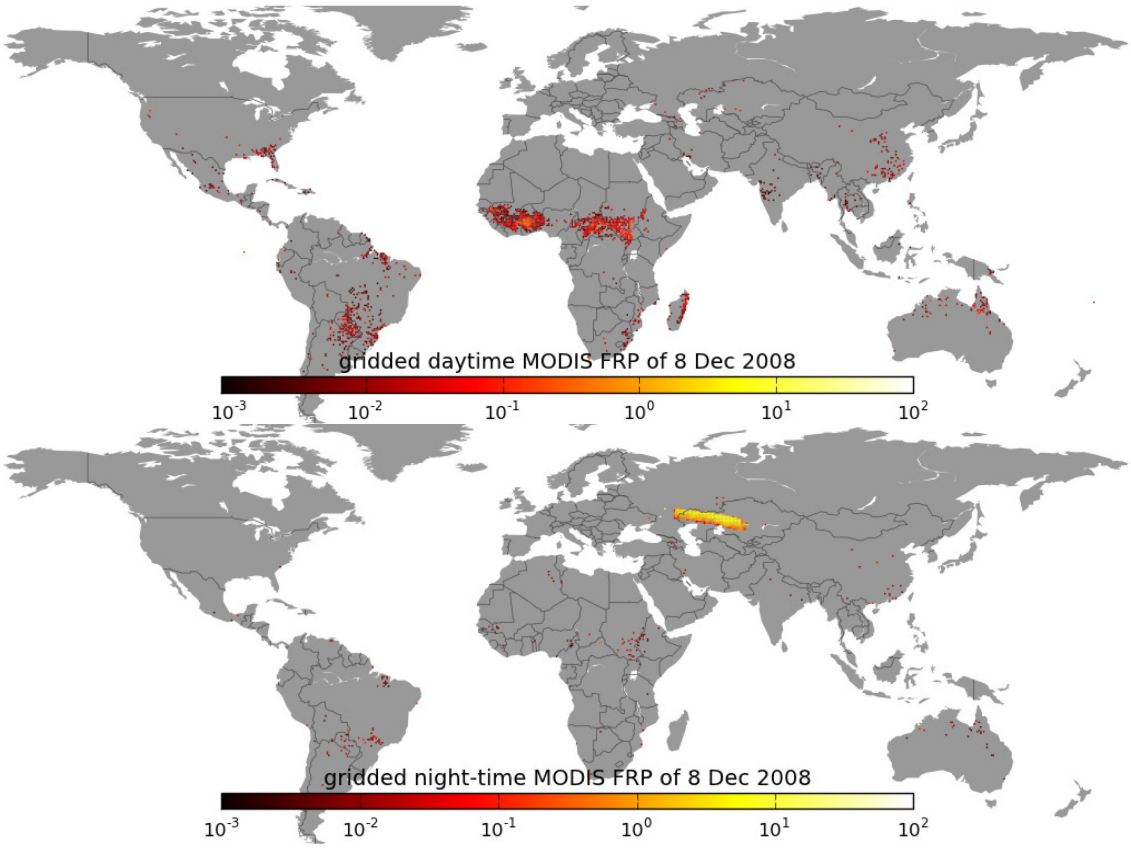

Figure 5.2: Gridded local daytime and night-time FRP observations of 8 Dec 2008 from the GFAS processing chain. The night-time observations feature an area of extremely high FRP values in the shape of a MODIS granule.

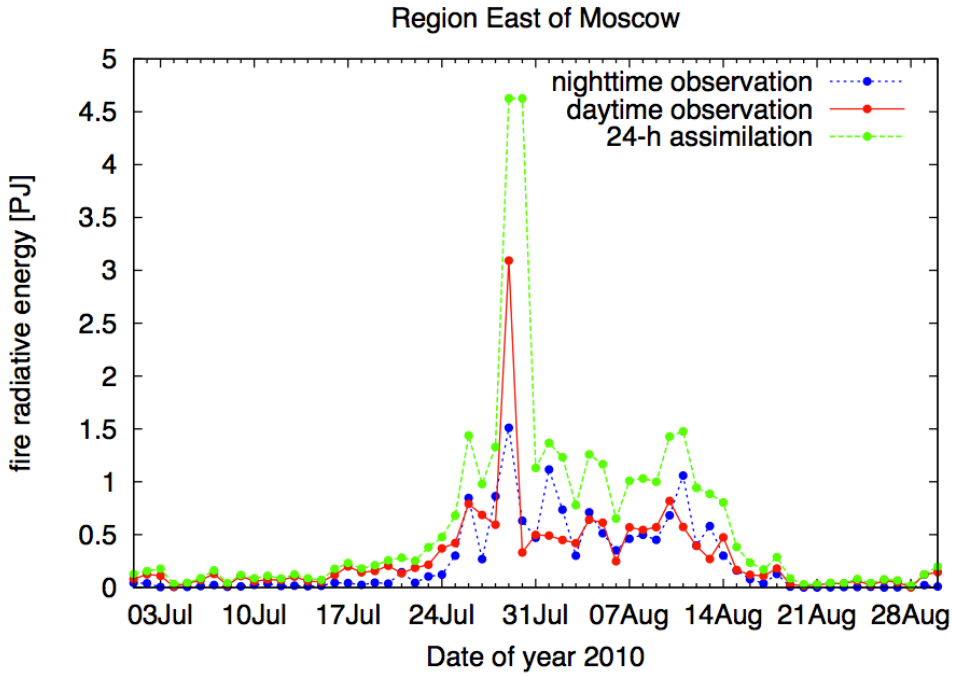

Figure 5.3: Temporal evolution of daytime and night-time FRE observations and the assimilated daily FRE from GFAS. ***From Kaiser et al. (2012).***

observations than just the suspicious ones obviously introduces additional and unnecessary uncertainties. In the future, only suspicious MODIS granules should be ignored and all other fire observations should be used in the FRP assimilation.

5.4 Masking of spurious signals

While the masking of signals from volcanoes, gas flares and industrial complexes appears to work generally very well, it should be updated because (*i*) the regions of Mediterranean Africa and the Middle East appear to have systematically larger emissions in GFAS than in other inventories, cf. Figure 2.5 and (*ii*) feedback from one reactive gas modeller in MACC-II indicates that spurious smoke plumes from industrial complexes in Central Europe are occasionally encountered in the global atmospheric model. In the long run, it may become possible to exploit the persistence of fire signals from such spurious sources to automatically flag them so that they can be added to the blacklist after manual inspection.

5.5 Peat fires

Peat fires are an important source of global emissions. These fires are difficult to detect by active fire satellite products because they partly burn below the surface. The comparison of GFED dry matter burned rates (DMb) with GFAS FRP showed that the effective FRP to DMb conversion factor is highest for peat (GFASv1.0 land cover class PEAT) and second highest for extratropical forests, which typically have a thick duff soil layer (GFASv1.0 land cover class EFOS; Heil et al., 2010; Kaiser et al., 2011). The effective conversion factor for fires in these major land cover classes is around 8 and 2 times, respectively, higher than for savanna fires, and at least 16 to 4 times higher, respectively, than the conversion factor given by Wooster et al. (2005). Peat (PEAT) and peaty soil/duff (OS) specific conversion factors (Heil et al., 2010) have been implemented in GFASv1.0 (Kaiser et al., 2012). Huijnen et al. (2011) demonstrated that for some regions, a good spatial representation of peat fires in GFAS is essential to accurately estimate emissions. Huijnen et al. (2011) analysed the quality of the forecasted tropospheric composition of various trace species emitted by the 2010 wildfires in western Russia. They found that GFASv1.0, with its explicit spatial representation of the peat areas of Western Russia (Figure 2.1a), showed good agreement with observations while GFASv0 and GFED3 - both having no peat areas in Western Russia - led to a significant underestimation.

Yet, the peat areas in GFASv1.0 are still constrained to Western Russia and Indonesia (Kalimantan and Sumatra), only, (Figure 5.2a) and cover a total area of around of 1.4 million km^2, and thus much less than the global estimate of peat areas of around 4 million km^2 by Joosten (2009). In the current GFASv1.0, for example, the vast peat areas in boreal North America are not represented. The omission of these peat areas may partly explain why CO emissions in GFAS in boreal North America are underestimated (see Section 2.2.1). Given this importance of peat soils for the quality of fire emission estimation, a substantial effort has been made towards an improvement of the spatial representation of peat soils in the GFAS dominant land cover type map.

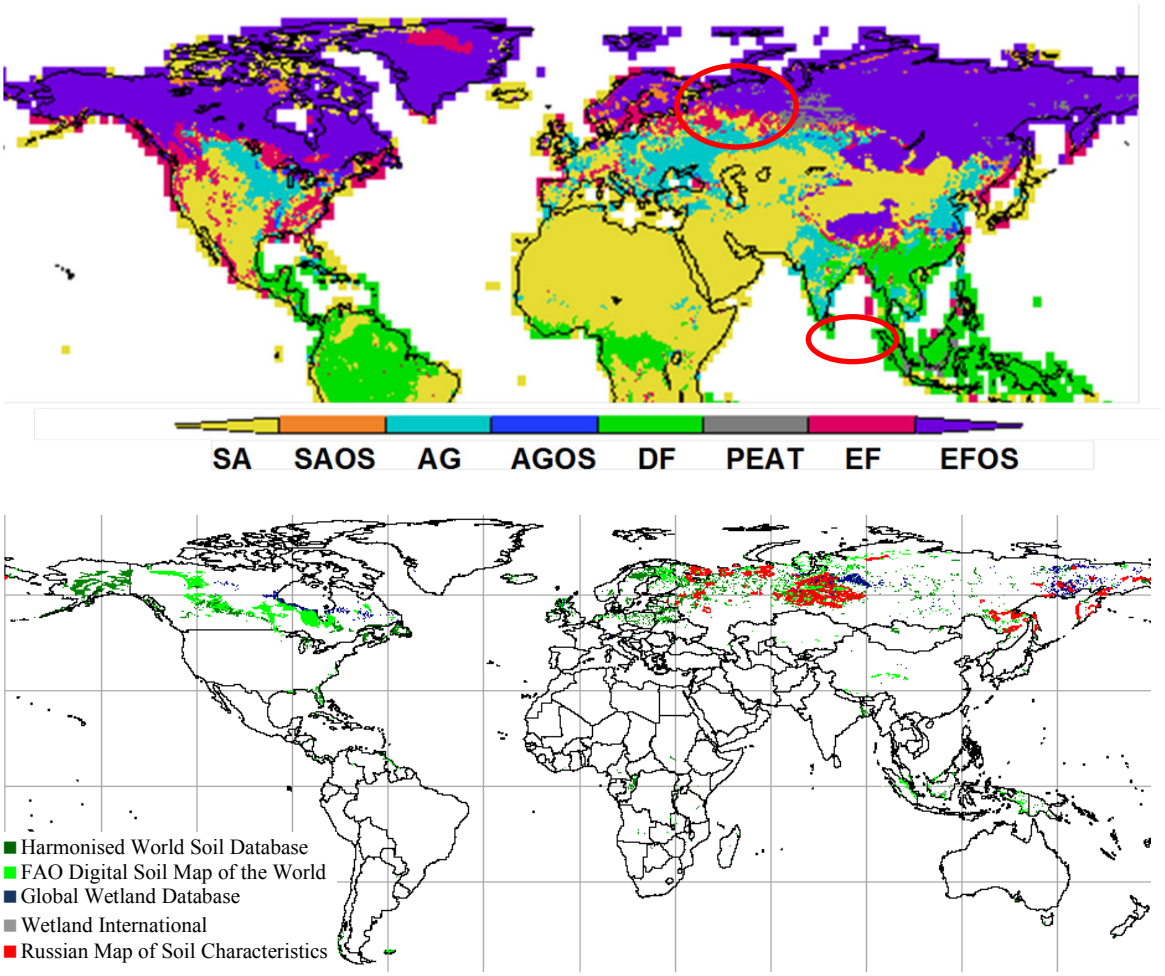

Figure 5.4: (a) GFASv1.0 predominant land cover type map with areas mapped as peat encircled in red (above) and (b) new GFASv2 preliminary map of the maximum area of potential peat burning. The colours indicate different map sources (see legend).

Several global and regional digital maps on the spatial distribution of soil groups and of soil organic carbon (SOC) exist. However, the spatial distribution and extent of soil groups and their respective soil properties vary greatly among the various maps, reflecting the large uncertainties of global soil inventories. Hiederer and Köchy (2011) summarised estimates of global SOC stocks (top 100 cm) from the most widely used global soil maps and demonstrated that SOC estimates range from 991 to 2470 Pg; thus they differ by up to 1500 Pg C, a number higher than the estimated carbon pools of the vegetation (610 Pg C) and the atmosphere (750 Pg C) together (IPCC, 1994). These uncertainties also affect estimates of soil matter burned.

Given the large differences in the representation of peat areas in the different soil maps, we investigated a composite approach where all areas identified as peat in at least one of five global or regional soil inventories are combined (Figure 5.1b). This map reflects the maximum area of potential peat burning, which is substantially higher than the extent of peat areas in the GFASv1.0 land cover map. Furthermore, it now includes the vast peat deposits occurring in boreal North America as well as peat areas in Eastern Europe and Scandinavia.

Further work is planned to discriminate between peat and non-peat fires within areas that are designated as peat in the combined soil type map. This can be achieved by exploiting typical characteristics of peat fires:

- Peat fires typically show a less pronounced diurnal cycle than other fires.
- Peat fires are relatively persistent and can burn for a consecutive number of days.
- The mean daily maximum FRP is typically relatively low for peat fires, because they are mostly burning below the subsurface, have lower temperatures and are mostly smouldering fires.

5.6 Emission Factors

The current version of GFAS relies on static emission factors that are based on the arithmetic mean of field measurements. Biome-averaged emission factors (EFs), compiled by Andreae and Merlet (2001) and updated by M.O. Andreae (Kaiser et al., 2012) were derived from measurements of fires in tropical forest, savanna and grassland, extratropical forest, tropical peat, and agricultural area. However, it is not known whether the available field measurement locations always provide a representative sample of the various biomes (van Leeuwen and van der Werf, 2011). For the extra-tropical forest biome for example, most of the EF measurements were conducted in boreal Alaska, and thus the biome-averaged EF is biased towards Alaska fires. In the more recent compilation of Akagi et al. (2011) the spatial variation of biome-averaged EFs increased: selected EFs for landscape-scale fires were organized into six types of vegetation (savanna, tropical forest, boreal forest, temperate forest, peatland, and chaparral). Thus, the category extratropical forest used by Andtrea and Merlet (2001) was divided into boreal and temperate forest, which may do justice to the differences between the fire characteristics for both biomes.

In addition to spatial variations, the EFs that are currently used in GFAS neglect temporal variability that is often found. Several studies have shown considerable variability of EFs throughout the year (Hoffa et al., 1999; Hely et al., 2003; Korontzi et al., 2003), and they linked this to substantial seasonality of different environmental parameters found in most biomass burning regions, and also to variation in EFs across vegetation and different fuel types (Meyer et al., 2012; Wooster et al., 2011). However, from a coarse resolution modeling perspective, exact relations between these parameters and the EFs cannot be extracted from the current body of literature (van Leeuwen and van der Werf, 2011). Van Leeuwen et al. (2013) showed that including EFs with different spatial and temporal variability in the GFED modeling framework has a significant impact on bottom-up emission estimates, and also on atmospheric mixing ratios. The large ranges of CO mixing ratios they found for boreal fires in 2003 and 2004 suggest that the contribution of EFs to this uncertainty is substantial, and may therefore explain part of the underestimation of CO emission estimates by GFED that was found by Yurganov et al. (2011) and Huijnen et al. (2011) for the intensive Russian wildfires in 2010. Differences to a static EF scenario of up to 50% were found for certain regions and time periods. A fuel type specific approach seemed to work better in the boreal areas, while including seasonality compared better to MOPITT measurements in South America. Besides more ground based measurements campaigns, an important step forward in our understanding of EF variability could be the setup of dedicated lab-experiments to test the role of different environmental parameters – like e.g. soil moisture, temperature, and wind – on EFs for different vegetation types.

Due to the substantial seasonality of different environmental parameters found in most biomass burning regions, dynamic EFs should be explored within the GFAS modeling framework. Also a fuel type specific approach (van Leeuwen et al., 2013) may be considered. Moreover, including the biome-averaged EF values of the more recent compilation of Akagi et al. (2011) could be useful: In contrast to the EF database of Andreae and Merlet (2001), Akagi et al. (2011) used EF measurements of 'fresh' smoke plumes only. These fresh plumes have cooled to ambient temperature, but have not yet undergone significant photochemical processing. Since chemical disturbances are therefore neglected, they may allow for a better representation of the true regional initial emissions of a fire, especially for short-lived compounds. Collaboration with the MACC-II colleagues who are modeling the reactive gases chemistry will be needed to ensure that the initial ageing of the smoke is appropriately represented.

Overall, we are relatively confident in the EFs of species where sufficient ground measurements are available, like for example CO. Although the temporal variation is hard to constrain from both bottom-up and top-down studies, and some measurements are lacking in important fire regions like Siberia, Central Africa, and Indonesia, we still feel that we are in the right order of magnitude for the EFs. However, for several other species - like e.g. NOx, BC, and $PM_{2.5}$ - uncertainty increases due to insufficient ground measurements and therefore a lack of information on seasonal and spatial variability. Therefore a continued focus on these species is needed in the validation activities of MACC-II and in future measurement campaigns.

In future, the potential for deriving estimates of biomass burning emissions ratios and perhaps emissions factors from atmospheric observations should be further investigated, based on the types of method detailed in Coheur et al. (2009). Atmospheric CO_2 enhancements due to biomass burning are difficult to retrieve due to the relatively small amounts by which the total CO_2 atmospheric column is enhanced in comparison to the high ambient atmospheric burden, but for species with a lower ambient mixing ratio (e.g. carbon monoxide, ammonia, formaldehyde etc.) this is not the case. The lack of a good quality CO_2 enhancement measure currently prevents the direct derivation of emissions factors from satellite atmospheric observations via the carbon mass balance technique (as used by e.g. Wooster et al., 2012 in ground-based emissions studies), but this may change in future with improvements in instruments (e.g. in spatial footprint size, and methods to directly target high concentration plumes). In the meantime, the possibilities for measuring plume emissions ratios of gases to e.g. CO should be further explored.

5.7 Fire activity forecasting

MACC-II produces daily forecasts of global atmospheric composition and European air quality with up to 5 days lead time. These model simulations have to assume smoke emission fluxes throughout their forecast period. Currently, no information on the evolution of detected fires is generated and the atmospheric systems assume persistence of the latest available GFAS emissions. This assumption is relatively well justified for regions with large and regular fire seasons (e.g. Africa), but less appropriate for the episodic fire behaviour in middle and higher latitudes. Huijnen et al. (2011) conclude that the persistence assumption "can lead to large overestimations of forecasted trace gas and aerosol concentrations when fire activity begins to subside after events of high emissions." They also recommend that "In order to avoid false pollution alarms, a more sophisticated approach to

forecast fire emissions based on the expected weather conditions and empirical analysis should be developed." An extreme example of such a potential false alarm for 2-4 August 2010 is illustrated in Figure 5.3.

The design of a "fire activity model" could dwell on a rich literature on fire danger forecasting, i.e. forecasting of the statistical distribution of fire activity, and would exploit well-known relationships between fire activity and meteorological parameters. For example, forest fires are fanned by strong winds and reduced by precipitation. However, the application of such principles to already ignited fires is a new scientific development.

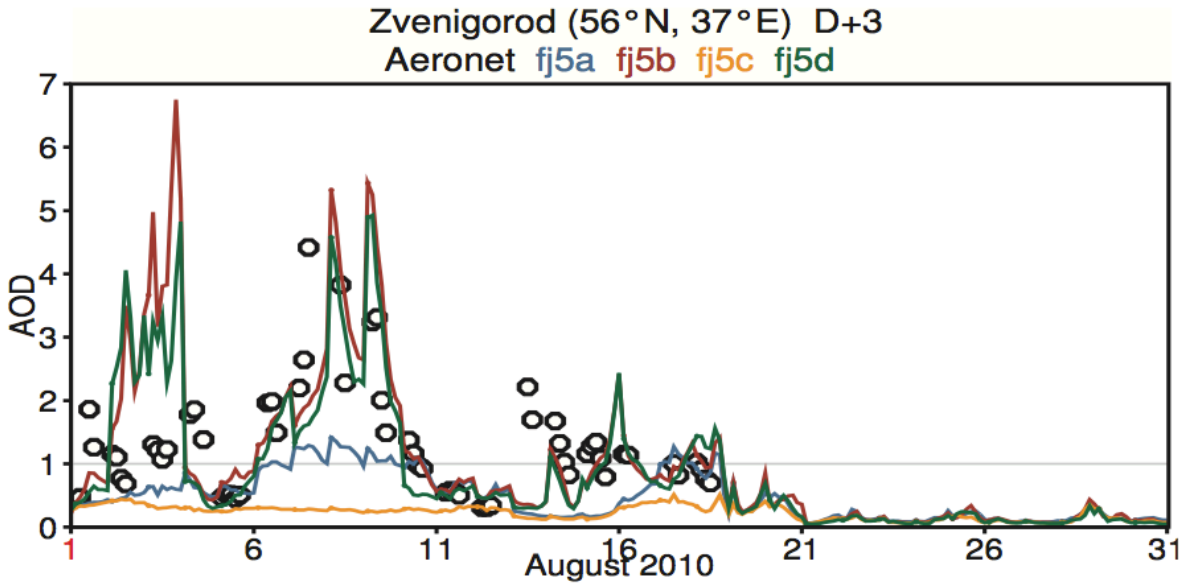

Figure 5.5: Hindcast experiments with 3 days lead time for aerosol optical depth in Zvenigorod near Moscow. Circles: AERONET observations. Red and green lines: simulations using GFAS emissions persisted from day 0. Blue and yellow: simulations using climatological fire emissions. ***From Kaiser et al. (2012)***

5.8 Injection Heights

The study of long-range transport of biomass burning emissions from Alaskan and Canadian fires in 2004 by Elguindi et al. (2010) found, that the plumes in the MACC reanalysis occur at the wrong altitude. This indicates wrong assumptions on the original injection heights of smoke from these fires.

Smoke plumes from vegetation fires rise in a smoke stack into upper layers of the atmosphere before being mixed with the ambient air. The plume rise depends on the properties of the fire, e.g. release of convective energy and size of the fire, and the ambient meteorological conditions, see, e.g. Freitas et al. (2007). Currently, the atmospheric systems in MACC need to decide themselves which injection height to assume for the fire emissions. However, a 1-d plume rise model is under development at King's College London (KCL). It uses ECMWF forecasts as meteorological input and is validated against MISR observations. This model will be included in GFAS, so that gridded, daily injection height information that applies for the actual fire situation can be made available to the atmospheric systems in the future.

5.9 Operational status

5.9.1 *Use of satellite data*

The GFAS emission estimates are derived from the two MODIS satellite instruments. These instruments still work faultlessly and the satellites carry consumables to last to about 2020. However, they are already beyond their expected lifetime and an instrument failure may always happen. In order to achieve sufficient resilience for an operational GFAS service, fire observations from more satellites need to be assimilated. FRP observations from two instruments on polar orbiting platforms will become available in the near future: VIIRS aboard Suomi NPP (launch in 2011, data availability expected during summer 2013) and SLSTR aboard Sentinel-3 (launch planned for 2014). Since both are operational satellites at the beginning of a series of identical or similar satellites, a continued availability of this input will be guaranteed. Assimilating FRP observations from the operational geostationary Meteosat-10 and GOES-East/-West satellites will strengthen the resilience of GFAS further. The suitability of FRP products from other geostationary satellites needs to be investigated once the first set of geostationary observations is successfully assimilated.

Currently, GFAS depends on the sampling of the diurnal variability of fires by the two MODIS instruments. Unavailability of observations from one of them would introduce a different sampling of the diurnal cycle of the fires and a bias in the fire emissions. This bias should be characterised at the global scale, so that it can be corrected immediately, if one of the MODIS instruments should cease its operations. In the longer term, such resilience should be built in for all assimilated satellite products. This will require reducing the temporal resolution to 1 hour and implementing an appropriate representation of the diurnal cycle.

5.9.2 *Computational environment*

Until now the GFAS experiments were not considered part of the operational tasks at ECMWF because it is a new development and because its products are immediately stored in the MARS archiving system, which is not considered operational. All other GFAS tasks are already performed on the operational High Performance Computing Facility (HPCF) at ECMWF. However, the data flow and model structures are rather different from the typical set-up of a weather model. Nevertheless, the production of GFAS has proven to be stable with delivery of the GFASv1.0 service within the planned 10-minute window on every day during a 31-day test period. The GFASv1.1 service was also delivered on 30 of these days during its anticipated 10-minute delivery window.

As a move towards a fully operational status, several modifications have already been implemented:

- Re-organisation of the model code so that a single experiment carries out all of the GFAS production.
- This single experiment produces both 0.5° (GFASv1.0) and 0.1° (GFASv1.1) data for FRE and compound emissions.
- The single experiment doesn't rely on archiving anymore in the production step.
- The code has been streamlined and computing efficiency improved.

As a result of these modifications, the GFAS experiment is now running within an infrastructure that possesses a set of statistics to measure the reliability of the system.

GFAS will need to run for a couple of months in this pre-operational setup, so that the pertinence of the timeliness and availability statistics can be assessed and a set of objectives determined. A documentation of the pre-operational GFAS can be found in annex B. GFAS will eventually become fully operational with the significant benefit of being monitored 24/7, and restarted in case any problem arises. Availability and timeliness statistics are also part of an experiment with operational status.

5.9.3 *Production schedule*

Requests for adaption of the timeliness and temporal resolution have been made by the global and regional MACC-II forecasting systems, respectively: The global atmospheric assimilation requires emission input that is specifically valid from 09UTC to 21UTC and from 21UTC to 09UTC. The regional systems require availability of emission products at 00UTC. An experimental version of GFAS has been successfully tested with an assimilation window of 24 hours running from 21 to 21UTC. This version will allow delivery of emission products a few hours sooner to the regional MACC-II forecasting system and is a step towards integration in the global atmospheric assimilation system.

5.10 Conclusions

The previous sections have shown that GFAS produces state-of-the-art fire emission estimates. However, the uncertainties of "state-of-the-art" are still large and should be reduced in the future in order to improve the accuracy of atmospheric composition air quality monitoring and forecasting. In this section, the several design aspects of GFAS that lead to uncertainties have been discussed.

With regard to FRP estimation, uncertainties arising from three aspects might be reduced:

- MODIS systematically underestimates the aggregate FRP near its swath edge.
- The fire diurnal cycle is not characterised in the daily GFAS product.
- The blacklisting of all observations from a 1-day time slot when the quality control detects dubious observation products in a 5-minute time slot of that day.
- Some spurious signals still escape the current spurious signal masking, especially in Northern Africa and the Near East.

Concerning the calculation of emissions based on FRP observations, most aspects were identified earlier by Heil et al. (2010) and are therefore not be repeated here. However, we note that:

- The current peat fire map is limited to Russia a uses only a single data source. These limitations may cause underestimations of regional emissions, especially in the boreal zones.
- Although good confidence exists in emission factors for common trace gases, emission factors of more rare trace gasses are often still relative uncertain. Until today, there is only limited understanding about the spatial and temporal variation of emission factors.

Within the MACC-II project GFAS aims not only to provide accurate real-time emission estimates but also to provide the required associated input data for the atmospheric modelling community. Therefore some model extensions are included or suggested:

- GFAS does not yet provide forecasts of fire activity and emissions. The current recommendation to assume fire persistence is a clear over-simplification.
- Injection heights of smoke plumes may have a large effect on initial distribution of trace gas concentrations and are currently not provided by GFAS.

Regarding operational status, GFAS already runs almost completely on operationally supported hardware, but:

- it still relies an archive that is not supported 24/7 and on observational input from just the two MODIS satellites.

6 Recommendations

GFAS provides robust near real-time global emission estimates for a wide range of trace gases. This is reflected by its growing user community and positive feedback provided by these operational and scientific groups: All global MACC-II systems use GFAS in real time and retrospectively, the first European air quality system, EURAD, uses GFAS in real time, the research branch of the Japanese Meteorological Agency uses GFAS in real time, and numerous scientific publications are based on GFAS data. In particular, GFAS appears to be relatively robust in regions with particular small fires and during episodes of exceptionally strong fires. Besides the current version GFASv1, GFAS is in continues development. In this report, we have assessed the quality of GFASv1. Here, recommendations considering the calculation of emissions from the FRP observations (Section 6.1), the actual satellite FRP observations (Section 6.2) and system extensions (Section 6.3) are discussed.

6.1 Emission calculation

Global emission inventories

Globally, a good comparison was found between three global emission inventories (GFAS, GFED and FINN). Relatively strong deviation was found regionally. Many differences between the emission inventories arise from the use of active fire or burned area products. GFAS emissions are scaled to meet average GFED emissions per biome, this causes good general agreement but regional differences remain. Conversion factors, used to convert FRP to DM burned calculated by GFED, are affected both by fire characteristics (e.g., fuel moisture content, fuel type, fire size) and unique product characteristics (e.g., ability to observe a fire, and observation angle). We recommend to carefully reconsider the conversion factors taking into account the different sources that may cause spatial distribution of conversion factors.

GFAS validation

GFAS emission estimates compared reasonably well with several case studies, although exceptions exist. Several studies show that GFAS emission estimates for boreal regions are on the low side, possibly caused by an underestimation of the emissions from peat fires. Commonly, GFAS emission estimates agreed better for some trace gases than for others. To better validate the performance of GFAS there is a need of more validation studies over important biomass burning regions, like the Arc of deforestation in South America, the African continent, and Equatorial Asia. The current literature is mainly focused on case studies in Russia and Greece, while large fire events in other parts of the

world are less well studied. For validation attempts in general, there is a need for more spatial and temporal overlap, and a step in the right direction could be the participation of MACC-II in large fire experiments where different bottom-up and models and validation methods (satellite, ground, aircraft) are combined. Moreover, species with a large uncertainty - due to a lack of measurements - that may play an important role in several atmospheric processes (like e.g. Black Carbon) should deserve more attention in future validation attempts.

Peat fires

Peat fires are an important source of global emissions and therefore need to be better incorporated in the GFAS product. In the current GFASv1.0 land cover map, the actual peat areas occurring globally are significantly underestimated, causing underestimation of peat fire emissions notably in boreal North America. A new map of peat regions has been developed and will be implemented in the next GFAS release. The GFAS map of potential areas with peat burning will be used to better characterize peat fires in GFAS and to improve conversion factors of biomes containing peat areas.

6.2 Underlying FRP estimation

MODIS observations

MODIS FRP observations are dependent on the viewing angle, causing an underestimation of gridded FRP near the swath edge. Although this effect is on average compensated for by conversion factors, it causes daily under and overestimations. Therefore, the associated systematic error of FRP observations with larger viewing angles should be characterised and compensated.

Temporal resolution

The fire diurnal cycle causes FRP observations to be of limited representativeness for the period of time until the next observation. As the diurnal cycle is observed from geostationary satellites, the time resolution of GFAS should be improved to 1hour and FRP products from geostationary satellites should also be assimilated. This will require a model or *a priori* assumptions for the diurnal cycle of fires in order to also operate in areas which are not observed from geostationary satellites. The improved time resolution will have the additional benefit that the GFAS products can satisfy the varying user requirements of validitiy periods and delivery times.

Operational status

The operational resilience should be improved by assimilating FRP products from the NPP-VIIRS and Sentinel-3-SLSTR instruments once they become available. This is in addition to the assimilation of geostationary FRP observations mentioned above. The relative bias of daily FRP products from the two MODIS instruments should be determined in order to be able to run GFAS with only one of the instruments for 2000-2002 and in case one of the instruments suddenly fails.

Other aspects

The GFAS quality control removes unrealistic observations but also introduces unnecessary uncertainties, therefore the quality control should be made more selective. Additionally it seems that although most spurious signals are masked out well, some remain in the actual GFAS product, we therefore recommend that the spurious signal mask should be updated.

6.3 System extension

Forecast of fire activity

Currently the atmospheric systems assume persistence of the latest GFAS emission estimate, while in reality this will depend on weather conditions and diurnal cycle. A global forecast of fire activity and emissions depending on the last observed fire activity, diurnal cycle and a meteorological forecast should be developed for a lead time of up to 5 days.

Injection height

The injection height has a large effect on initial distribution of smoke plumes, therefore global estimates of the injection height distribution depending on fire observations and meteorological analyses and forecasts should be made available based on the existing developments at KCL.

7 References

Akagi, S. K., Yokelson, R. J., Wiedinmyer, C., Alvarado, M. J., Reid, J. S., Karl, T., Crounse, J.D., and P. O. Wennberg (2011). Emission factors for open and domestic biomass burning for use in atmospheric models. *Atmospheric Chemistry and Physics*, 11(9), 4039-4072.

Al-Saadi, J., Soja, A. J., Pierce, R. B., Szykman, J., Wiedinmyer, C., Emmons, L., Kondragunta, S., Zhang, X., Kittaka, C., Schaack, T., and K. Bowman (2008). Intercomparison of near-real-time biomass burning emissions estimates constrained by satellite fire data. *Journal of Applied Remote Sensing*, 2(1), 021504-021504.

Andreae, M. O., and Merlet, P. (2001). Emission of trace gases and aerosols from biomass burning. *Global biogeochemical cycles*, 15(4), 955-966.

Chevallier, F., A. Fortems, P. Bousquet, I. Pison, S. Szopa, M. Devaux, and D. A. Hauglustaine (2009). African CO emissions between years 2000 and 2006 as estimated from MOPITT observations. *Biogeosciences,* 6(1): 103-111.

Christian, T. J., Kleiss, B., Yokelson, R. J., Holzinger, R., Crutzen, P. J., Hao, W. M., Saharjo, B.H., and D. E. Ward (2003). Comprehensive laboratory measurements of biomass-burning emissions: 1. Emissions from Indonesian, African, and other fuels. *Journal of Geophysical Research*, 108(D23), 4719.

Coheur, P., L., Clarisse, S., Turquety, D., Hurtmans, and C. Clerbaux (2009). IASI measurements of reactive trace species in biomass burning plumes. *Atmospheric Chemistry and Physics*, 9(15), 5655–5667.

Detmers, R. G., and G. R. van der Werf (2013). Fuel consumption rates for biomass burning: A field measurement database. In preparation.

Edwards, D. P., Emmons, L.K., Hauglustaine, D. A., Chu, D. A., Gille, J. C., Kaufman, Y. J., Pétron, G., Yurganov, L. N., Giglio, L., Deeter, M. N., Yudin, V., Ziskin, G., Francis, L., Ho, S. P., Mao, D. Chen, J. Grechko, E. L., and J. R. Drummond (2004). Observations of carbon monoxide and aerosols from the Terra satellite: Northern Hemisphere variability. *Journal of Geophysical Research*, 109, D24202, doi:10.1029/2004JD004727.

Elguindi, N., H. Clark, C. Ordóñez, and V. Thouret (2010). Current status of the ability of the GEMS/MACC models to reproduce the tropospheric CO vertical distribution as measured by MOZAIC. *Geoscientific Model Development*, 3, 501-518. doi:10.5194/gmd-3-501-2010.

Fokeeva, E. V., A. N. Safronov, V. S. Rakitin, L. N. Yurganov, E. I. Grechko, and R. A. Shumskii (2011). Investigation of the 2010 July–August fires impact on carbon monoxide atmospheric pollution in Moscow and its outskirts, estimating of emissions, Izvestiya. *Atmospheric and Oceanic Physics*, 47(6), 682–698, doi:10.1134/S0001433811060041.

Fortems-Cheiney, A., F. Chevallier, I. Pison, P. Bousquet, S. Szopa, M. N. Deeter, and C. Clerbaux (2011). Ten years of CO emissions as seen from Measurements of Pollution in the Troposphere (MOPITT). *Journal of Geophysical Research*, 116, D05304, doi:10.1029/2010JD014416.

Freitas, S.R., K. M. Longo, R. Chatfield, D. Latham, M. A. F. Silva Dias, M. O. Andreae, E. Prins,J. C. Santos, R. Gielow, and J. A. Carvalho Jr. (2007). Including the sub-grid scale plume rise of vegetation fires in low resolution atmospheric transport models. *Atmospheric Chemistry and Physics*, 7: 3385-3398.

Giglio, L., Van Der Werf, G. R., Randerson, J. T., Collatz, G. J., & Kasibhatla, P. (2005). Global estimation of burned area using MODIS active fire observations. *Atmospheric Chemistry and Physics Discussions*, 5(6), 11091-11141.

Giglio, L. (2007). Characterization of the tropical diurnal fire cycle using VIRS and MODIS observations. *Remote Sensing of Environment*, 108(4), 407-421.

Giglio, L., Randerson, J. T., van der Werf, G. R., Kasibhatla, P. S., Collatz, G. J., Morton, D. C., and R.S. De Fries (2010). Assessing variability and long-term trends in burned area by merging multiple satellite fire products. *Biogeosciences*, 7, 1171-1186, doi:10.5194/bg-7-1171-2010.

Gloudemans, A. M. S., M. C. Krol, J. F. Meirink, A. T. J. de Laat, G. R. van der Werf, H. Schrijver, M. M. P. van den Broek, and I. Aben (2006). Evidence for long-range transport of carbon monoxide in the Southern Hemisphere from SCIAMACHY observations. *Geophysical Research Letters*, 33, L16807, doi:10.1029/2006GL026804.

Gonzi, S., L. Feng, and P. I. Palmer (2011). Seasonal cycle of emissions of CO inferred from MOPITT profiles of CO: Sensitivity to pyroconvection and profile retrieval assumptions. *Geophysical Research Letters*, 38, L08813, doi:10.1029/2011GL046789.

Heil, A., Kaiser, J. W., van der Werf, G. R., Wooster, M. J., Schultz, M. G., and D. H. van der Gon (2010). Assessment of the Real-Time Fire Emissions (GFASv0) by MACC. Tech. Memo. 628, ECMWF, Reading, UK.

Hely, C., S. Alleaume, R. J. Swap, H. H. Shugart, and C. O. Justice (2003). SAFARI-2000 characterization of fuels, fire behavior, combustion completeness, and emissions from experimental burns in infertile grass savannas in western Zambia. *Journal of Arid Environments*, 54(2), 381–394, doi:10.1006/jare.2002.1097.

Hiederer, R. and Köchy, M. (2012). Global Soil Organic Carbon Estimates and the Harmonized World Soil Database. *EUR Scientific and Technical Research series*, doi:10.2788/13267.

Hoelzemann, J. J., Schultz, M. G., Brasseur, G. P., Granier, C., and M. Simon (2004). Global Wildland Fire Emission Model (GWEM): Evaluating the use of global area burnt satellite data. *Journal of Geophysical Research*, 109(D14), D14S04.

Hoffa, E. A., D. E. Ward, W. M. Hao, R. A. Susott, and R. H. Wakimoto (1999). Seasonality of carbon emissions from biomass burning in a Zambian savanna. *Journal of Geophysical Research-Atmospheres*, 104, 13841–13853.

Hooghiemstra, P. B., M. C. Krol, J. F. Meirink, P. Bergamaschi, G. R. Van Der Werf, P. C. Novelli, I. Aben, and T. Röckmann (2011). Optimizing global CO emission estimates using a four-dimensional variational data assimilation system and surface network observations. *Atmospheric Chemistry and Physics*, 11(10), 4705–4723, doi:10.5194/acp-11-4705-2011.

Hooghiemstra, P. B., M. C. Krol, P. Bergamaschi, A. T. J. de Laat, G. R. van der Werf, P. C. Novelli, M. N. Deeter, I. Aben, and T. Röckmann (2012). Comparing optimized CO emission estimates using MOPITT or NOAA surface network observations. *Journal of Geophysical Research*, 117, D06309, doi:10.1029/2011JD017043.

Huang, S., F. Siegert, J. G. Goldammer, and A. I. Sukhinin (2009). Satellite-derived 2003 wildfires in southern Siberia and their potential influence on carbon sequestration. *International Journal of Remote Sensing*, 30(6), 1479–1492, doi:10.1080/ 01431160802541549.

Huijnen V, Flemming J, Kaiser J. W., Inness A, Leitao J., Heil, A., Eskes, H. J., Schultz M. G., Benedetti, A., Dufour, G., and M. Eremenko (2011). Hindcast experiments of tropospheric composition during the summer 2010 fires over Western Russia. *Atmospheric Chemistry and Physics*. 11:31851–31909. doi:10.5194/acpd-11-31851-2011.

Huneeus, N., F. Chevallier, and O. Boucher (2012). Estimating aerosol emissions by assimilating observed aerosol optical depth in a global aerosol model. *Atmospheric Chemistry and Physics*, 12(10), 4585–4606, doi:10.5194/acp-12-4585-2012.

Inness, A., Baier, F., Benedetti, A., Bouarar, I., Chabrillat, S., Clark, H., Clerbaux, C., Coheur, P., Engelen, R. J., Errera, Q., Flemming, J., George, M., Granier, C., Hadji-Lazaro, J., Huijnen, V., Hurtmans, D., Jones, L., Kaiser, J. W., Kapsomenakis, J., Lefever, K., Leitão, J., Razinger, M., Richter, A., Schultz, M. G., Simmons, A. J., Suttie, M., Stein, O., Thépaut, J.-N., Thouret, V., Vrekoussis, M., Zerefos, C., and the MACC team (2013). The MACC reanalysis: an 8-yr data set of atmospheric composition. *Atmospheric Chemistry and Physics*, 13, 4073-4109, doi:10.5194/acp-13-4073-2013.

Intergovernmental Panel on Climate Change (IPCC) (Houghton, J. T., Meira Filho, L. G., Bruce, J., Hoesung Lee, Callander, B. A., Haites, E., Harris, N. and Maskell, K. (eds) (1994). Radiative Forcing of Climate Change and an Evaluation of IPCC IS92 Emission Scenarios. *Cambridge University Press*, Cambridge, UK, 199, pp. 339.

Ito, A., & Penner, J. E. (2004). Global estimates of biomass burning emissions based on satellite imagery for the year 2000. *Journal of Geophysical Research*, 109(D14), D14S05.

Jones, D. B. A., K. W. Bowman, J. A. Logan, C. L. Heald, J. Liu, M. Luo, J. Worden, and J. Drummond (2009). The zonal structure of tropical O3 and CO as observed by the Tropospheric

Emission Spectrometer in November 2004–Part 1: Inverse modeling of CO emissions. *Atmospheric Chemistry and Physics,* 9(11): 3547-3562.

Joosten, H. (2009). The global peatland CO_2 picture. Peatland status and drainage related emissions in all countries of the world. *Wetlands International*.

Kaiser, J. W., Heil, A., Andreae, M. O., Benedetti, A., Chubarova, N., Jones, L., Morcrette, J. J., Razinger, M., Schultz, M. G., Suttie, M., and G. R. van der Werf (2012). Biomass burning emissions estimated with a global fire assimilation system based on observed fire radiative power. *Biogeosciences*, 9(1), 527-554.

Konovalov, I. B., M. Beekmann, I. N. Kuznetsova, A. Yurova, and A. M. Zvyagintsev (2011). Atmospheric impacts of the 2010 Russian wildfires: integrating modelling and measurements of an extreme air pollution episode in the Moscow region. *Atmospheric Chemistry and Physics*, 11(19), 10031–10056, doi:10.5194/acp-11-10031-2011.

Kopacz, Monika, D. J. Jacob, J. A. Fisher, J. A. Logan, Lin Zhang, I. A. Megretskaia, R. M. Yantosca, Singh, K., Henze, D. K., Burrows, J. P., Buchwitz, M., Khlystova, I., McMillan, W. W., Gille, J. C., Edwards, D. P., Eldering, A., Thouret, V., and P. Nedelec (2010). Global estimates of CO sources with high resolution by adjoint inversion of multiple satellite datasets (MOPITT, AIRS, SCIAMACHY, TES). *Atmospheric Chemistry and Physics* 10(3), 855-876.

Korontzi, S., D. E. Ward, R. A. Susott, R. J. Yokelson, C. O. Justice, P. V. Hobbs, E. Smithwick, and W. M. Hao (2003). Seasonal variation and ecosystem dependence of emission factors for selected trace gases and PM2.5 for southern African savanna fires. *Journal of Geophysical Research-Atmospheres*, *108*, 4758, doi:10.1029/2003JD003730.

Krol, M., Peters, W., Hooghiemstra, P., George, M., Clerbaux, C., Hurtmans, D., McInerney, D., Sedano, F., Bergamaschi, P., El Hajj, M., Kaiser, J. W., Fisher, D., Yershov, V., and J. P. Muller (2012). How much CO was emitted by the 2010 fires around Moscow? *Atmospheric Chemistry and Physics*, 12, 28705-28731, doi:10.5194/acpd-12-28705-2012, 2012.

Lammel, G., Heil, A., Stemmler, I., Dvorská, A., Klánová, J. (2013). On the contribution of biomass burning to POPs (PAHs and PCDDs) in air in Africa. Submitted to *Environmental Science & Technology*.

Van Leeuwen, T. T., and G. R. Van Der Werf (2011). Spatial and temporal variability in the ratio of trace gases emitted from biomass burning. *Atmospheric Chemistry and Physics*, 11(8), 3611–3629, doi:10.5194/acp-11-3611-2011.

Van Leeuwen, T. T., W. Peters, M. C. Krol, and G. R. Van Der Werf (2013). Dynamic biomass burning emission factors and their impact on atmospheric CO mixing ratios. *Journal of Geophysical Research – Atmospheres*, accepted.

Mack, M. C., M. S. Bret-Harte, T. N. Hollingsworth, R. R. Jandt, E. A. G. Schuur, G. R. Shaver, and D. L. Verbyla (2011). Carbon loss from an unprecedented Arctic tundra wildfire. *Nature*, 475(7357), 489–492, doi:10.1038/nature10283.

Melas D., E. Katragkou, M. Schulz, K. Lefever, V. Huijnen, and H. Eskes (eds.), Validation report of the MACC reanalysis of global atmospheric composition: Period 2003-2011, MACC II Validation Report, EU MACC II project, 2013.

Meyer, C. P., G. D. Cook, F. Reisen, T. E. L. Smith, M. Tattaris, J. Russell-Smith, S. W. Maier, C. P. Yates, and M. J. Wooster (2012). Direct measurements of the seasonality of emission factors from savanna fires in northern Australia. *Journal of Geophysical Research*, *117*(D20), D20305, doi:10.1029/2012JD017671.

Pfister, G., P. G. Hess, L. K. Emmons, J. F. Lamarque, C. Wiedinmyer, D. P. Edwards, G. Pétron, J. C. Gille, and G. W. Sachse (2005). Quantifying CO emissions from the 2004 Alaskan wildfires using MOPITT CO data. *Geophysical Research Letters*, 32(11), L11809, doi:10.1029/2005GL022995.

Pison, I., P. Bousquet, F. Chevallier, S. Szopa, and D. Hauglustaine (2009). Multi-species inversion of CH4, CO and H2 emissions from surface measurements. *Atmospheric Chemistry and Physics* 9(14), 5281-5297.

Potter, C. S., Randerson, J. T., Field, C. B., Matson, P. A., Vitousek, P. M., Mooney, H. A., and S. A. Klooster (1993). Terrestrial ecosystem production: a process model based on global satellite and surface data. *Global Biogeochemical Cycles*, *7*(4), 811-841.

Randerson, J. T., Y. Chen, van der Werf, G. R., Rogers, B. M., *and* D. C. Morton *(*2012*)*. Global burned area and biomass burning emissions from small fires. *Journal of Geophysical Research,* 117*, G04012.*

van der Werf, G. R., Randerson, J. T., Giglio, L., Collatz, G. J., Mu, M., Kasibhatla, P. S., Morton, D. C., DeFries, R. S., Jin, Y., and T. T. van Leeuwen (2010). Global fire emissions and the contribution of deforestation, savanna, forest, agricultural, and peat fires (1997–2009). *Atmospheric Chemistry and Physics*, *10*(23), 11-707.

Wiedinmyer, C., Quayle, B., Geron, C., Belote, A., McKenzie, D., Zhang, X., O'Neill, S., and K. K., Wynne (2006). Estimating emissions from fires in North America for air quality modeling. *Atmospheric Environment*, *40*(19), 3419-3432.

Wiedinmyer, C., Akagi, S. K., Yokelson, R. J., Emmons, L. K., Al-Saadi, J. A., Orlando, J. J., and A. J. Soja (2011). The Fire INventory from NCAR (FINN): a high resolution global model to estimate the emissions from open burning. *Geoscientific Model Development*, 4, 625–641, doi: 10.5194.

Wooster, M. J., Roberts, G., Perry, G. L. W., and Y. J. Kaufman (2005). Retrieval of biomass combustion rates and totals from fire radiative power observations: FRP derivation and calibration relationships between biomass consumption and fire radiative energy release. *Journal of Geophysical Research*, 110, D24311.

Wooster, M. J., P. H. Freeborn, S. Archibald, C. Oppenheimer, G. J. Roberts, T. E. L. Smith, N. Govender, M. Burton, and I. Palumbo (2011). Field determination of biomass burning emission ratios and factors via open-path FTIR spectroscopy and fire radiative power assessment: headfire, backfire and residual smouldering combustion in African savannahs. *Atmospheric Chemistry and Physics*, 11(22), 11591–11615, doi:10.5194/acp-11-11591-2011.

Stolbovoi, V. and Savin, I.: Maps of soil characteristics. In Stolbovoi V. and I. McCallum, eds. Land resources of Russia. Laxenburg, Austria: International Institute for Applied Systems Analysis

and the Russian Academy of Science. CD-ROM. Distributed by the National Snow and Ice Data Center, Boulder, 2002.

Turquety, S., J. A. Logan, and D. J. Jacob (2007). Inventory of boreal fire emissions for North America in 2004: Importance of peat burning and pyroconvective injection. *Journal of Geophysical Research*, 112, D12S03, doi:10.1029/2006JD007281.

Turquety, S., D. Hurtmans, J. Hadji-Lazaro, P. F. Coheur, C. Clerbaux, D. Josset, and C. Tsamalis (2009). Tracking the emission and transport of pollution from wildfires using the IASI CO retrievals: analysis of the summer 2007 Greek fires. *Atmospheric Chemistry and Physics*, 9, 4897–4913.

Yurganov, L. N., Rakitin, V., Dzhola, A., August, T., Fokeeva, E., George, M., George, M., Gorchakov, G., Grechko, E., Hannon, S., Karpov, A., Ott, L., Semutnikova, E., Shumsky, R., and L. Strow (2011). Satellite- and ground-based CO total column observations over 2010 Russian fires: accuracy of top-down estimates based on thermal IR satellite data. *Atmospheric Chemistry and Physics*, *11*(15), 7925-7942.

A. Annex material

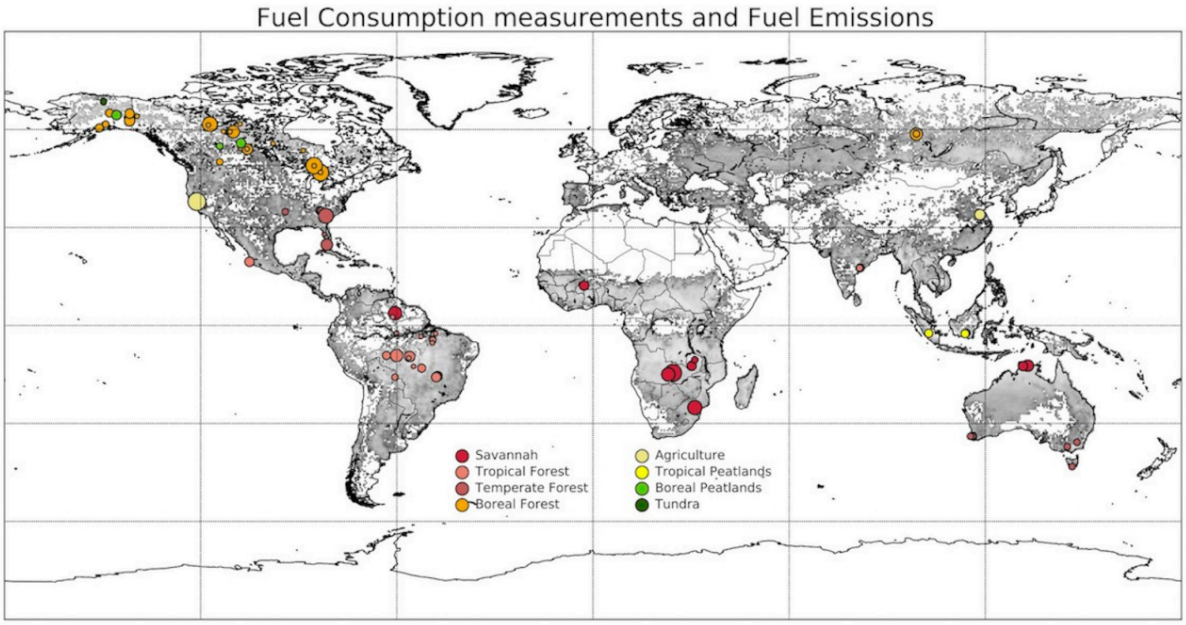

Figure A. 1: Distribution of fuel consumption studies, where larger circles indicate several measurements are made at the same location. ***From Detmers and van der Werf, in progress****.*

B. Documentation of the "pre-operational" GFAS

Table of contents

I. Overview

Biomass fires are a prominent source of tropospheric aerosols, green-house and trace gases. The Global Fire Assimilation System (GFAS) is a data assimilation system which produces daily analyses of Fire Radiative Power (FRP) and of the emissions of aerosols and 41 trace gases caused by biomass burning. It uses remote data from MODIS on Aqua and Terra (see Kaiser et al., 2012 for more details on the scientific basis of GFAS).

This document aims to show in detail how the pre-operational GFAS system works on the ecgems server. The GFAS experiment is currently fvbb, running in near real-time mode or delayed mode.

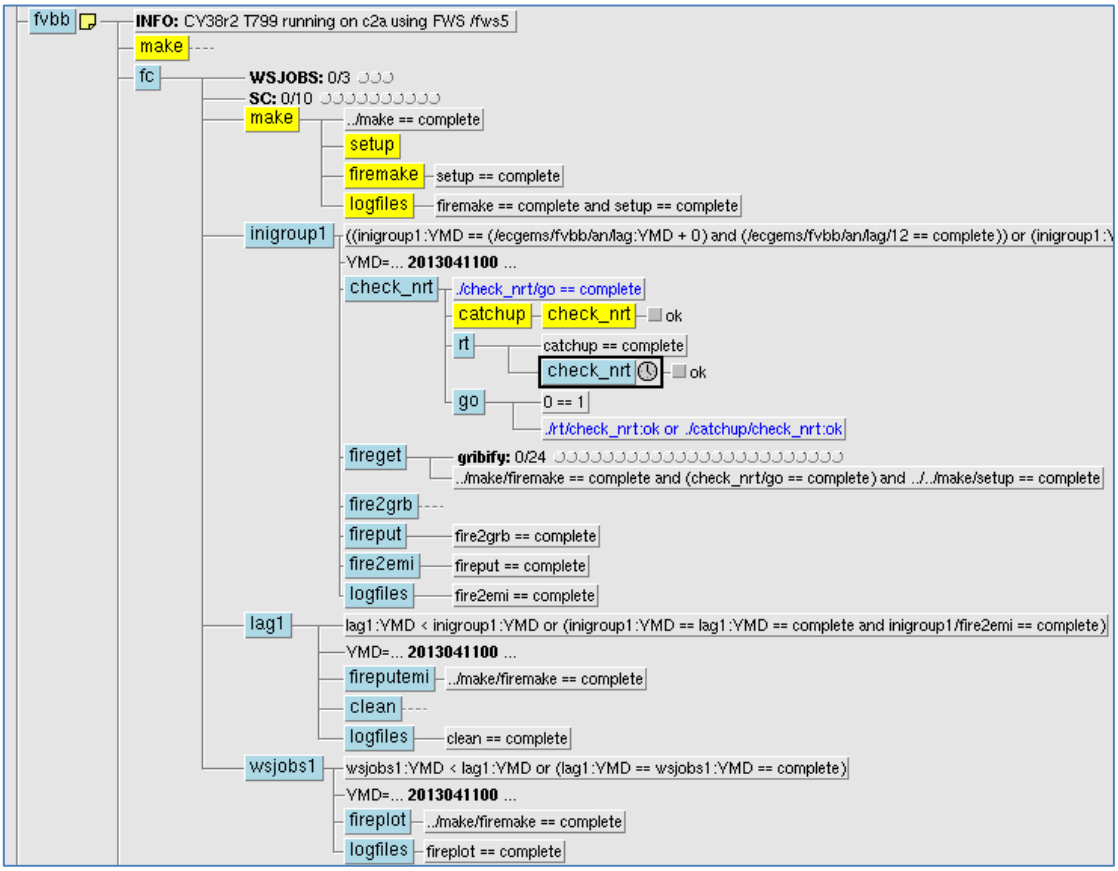

Figure B. 1: the different tasks of the pre-operationl GFAS experiment fvbb

As shown by Figure B. 1, GFAS consists of the following tasks:

- Firemake is the first script to be launched. It copies data and script files, prepares for the interpolation of the output that takes place in the fireputemi script and compiles the C and Fortran sources that are used in the firedo script. It is run only once.
- Loop over a family of dates that is defined in prepIFS. In the current setup, GFAS is run every 24 hours to assimilate Fire Radiative Power (FRP) from 0 to 0UTC includes the following tasks :
    - The check_nrt task, which checks the base time against the date to determine whether GFAS is run in Near Real Time (NRT) mode or delayed mode. For NRT time, GFAS for a given day is launched the following day at 5am.

- the fireget task which fetches the data from MODIS on Aqua and Terra,
- 24 firedo tasks, that grid the 5mn MODIS FRP data for one hour interval each :

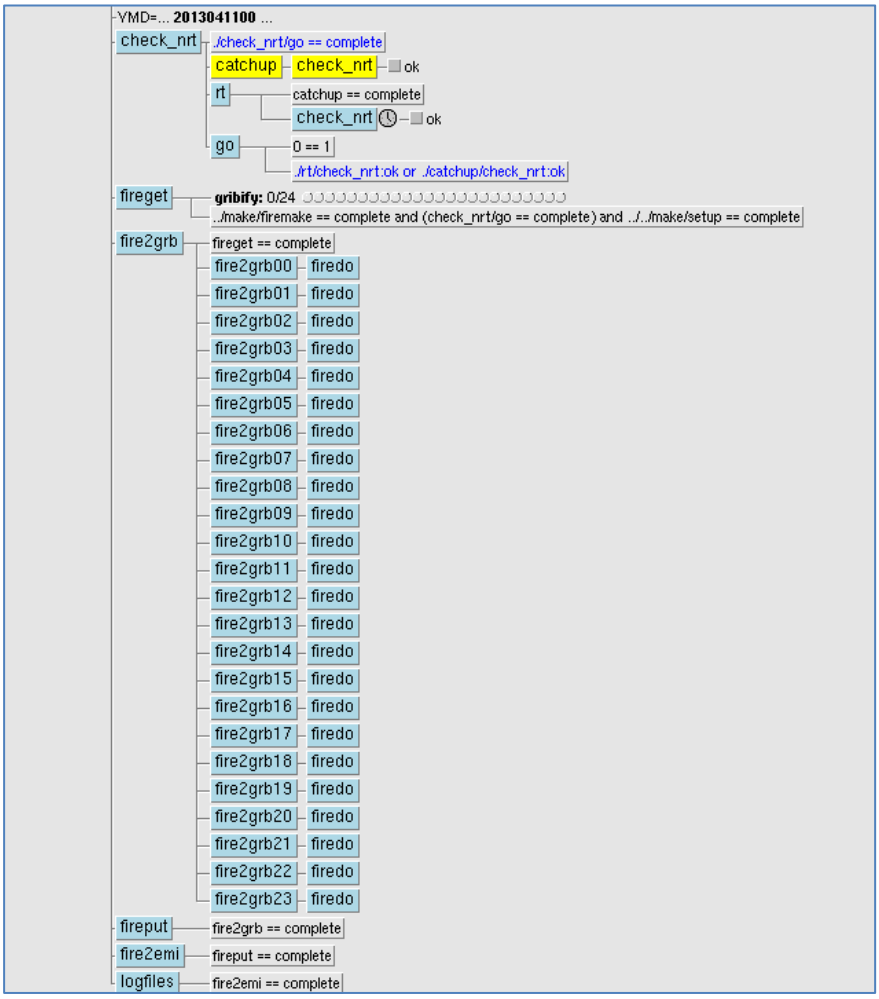

Figure B. 2: Gridding the satellite data in GFAS by the 24 firedo tasks

- The fireput task that averages the FRP data over one hour intervals
- The fire2emi task that assimilates the FRP data (with a Kalman filter using persistence as the forecast step) and then translates FRP into emissions for 41 species.

- Another loop over the same dates has been added for jobs that can lag behind :
  - The fireputemi job that archives FRP analysis, emissions and gridded satellite data into MARS
  - The clean task that removes the working directories
- Another loop over the same dates has been added for jobs that are run on the work station :
  - The fireplot task creates the KML files of the FRP analysis

GFAS uses data from various satellites to compute a daily analysis of FRP and trace gases emissions. These satellites are defined in the "FRP_SAT" variable that is set in fc.def. Each satellite is separated by a "_" symbol in this variable, which currently holds the following value: "MODISAqua_MODISTerra". As of today, only MODIS on Aqua and Terra are used in GFAS. The following values are possible in the "FRP_SAT" variable (case sensitive):

- MODISAqua
- MODISTerra
- SEVIRI
- GoesE
- GoesW

II. Directory structure of GFAS on the supercomputer

In the root directory of the fvpp experiment on the supercomputer (/fws5/lb/work/rd/ecgems/fvbb/), there are three directories and one file that are used by GFAS:

- the corruptproducts file that contains entries for each satellite product that couldn't be correctly decoded by GFAS,
- The bin directories contains the executables (python or compiled from C or Fortran90) used by GFAS,
- The dat directory that contains the constant data fields used by GFAS :
  - The land-sea mask
  - The null FRP grib field
  - Gas flares data
  - Land cover map to translate FRP into dry matter combustion rate
  - CDO 0.1° to 0.5° remapping weight template
  - Analysis of daily FRP produced by GFAS, to be used in the assimilation process.
- The working directory, in the form of YYYYMMDD00/gfc. This directory is deleted by the clean task (see above) at the end of the loop of lagged jobs. It contains the following sub-directories :
  - raw, which contains the raw data from MODIS/Aqua and MODIS/Terra.
  - tmpHH, which are the working directories for the gridding of the MODIS data from HH+00 to HH+55mn
  - grb, containing the final 5mn gridded MODIS data

The following files are also in the working directory:

  - the average hourly and daily gridded MODIS FRP data for each satellite, output of the fireput script (hourly*.grb and daily*.grb)
  - The daily analysis of FRP (frp_archive*.grb) and the associated emissions of trace gases (emi_archive*.grb) for 0.1° and 0.5°. 0.1° and 0.5° data are kept in separate files.

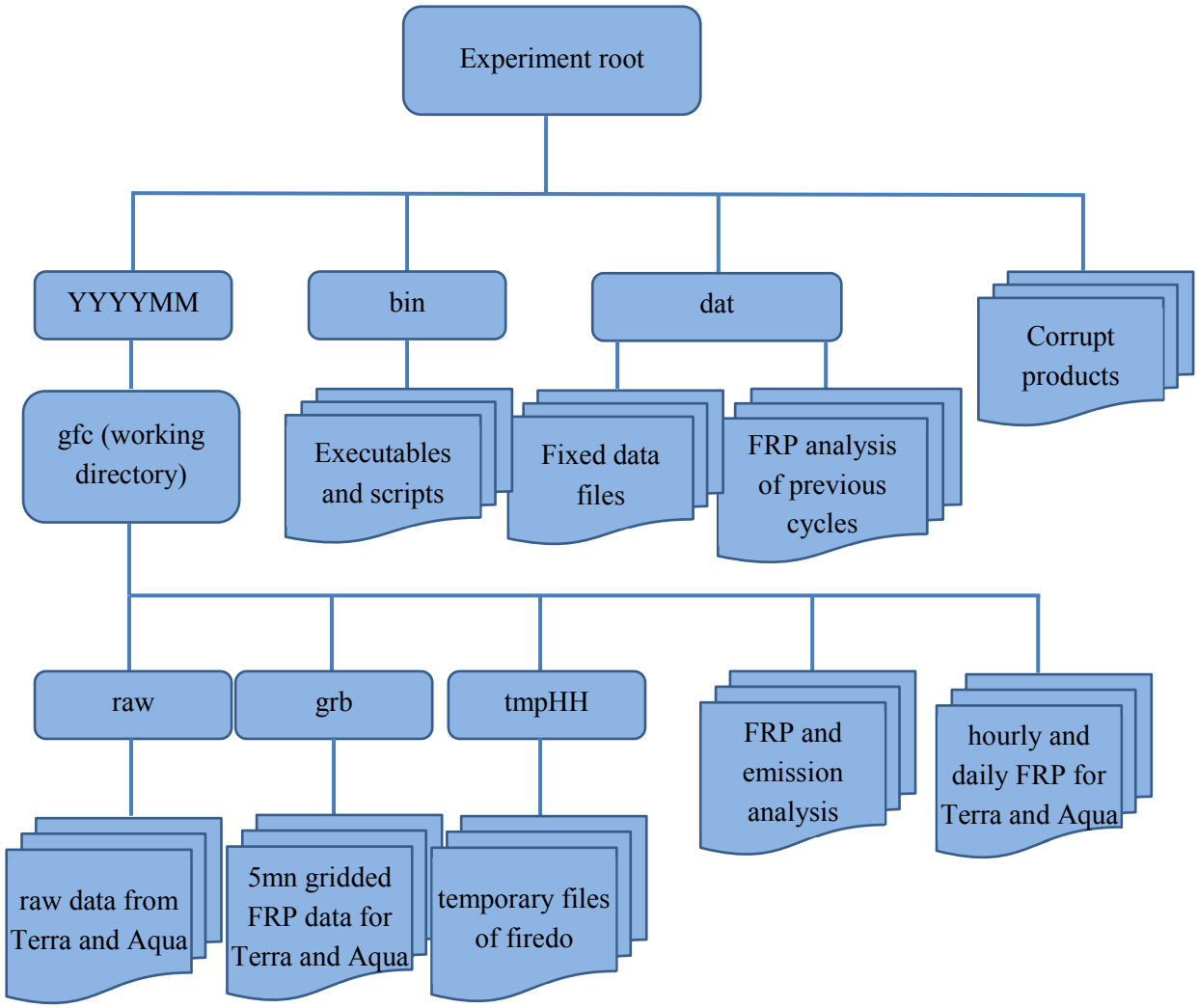

Figure B. 3: Directory structure of GFAS

III. Setup and Compilation: firemake

Firemake copies and compiles files that are originally in the ~disr directory of C2A. The files are copied into various subdirectories of the working directory (see above). The sequence of operations is:

- Copy of the land-sea mask, the no-observation grib files, the land cover and of the gas flare files into the "dat" sub-directory of the working directory
- Creation of the CDO remapping weight template using a 0.1° analysis of FRP and a CDO configuration file.
- Copy of python and shell scripts
- Copy of C and fortran90 sources and compilation using cc, pgf90 and hdf libraries (for both C and Fortran)

IV. Fetching the data: fireget

Fireget fetches the raw data from the satellites defined by the "FRP_SAT" variable (see Overview for more details).

A loop is done over these satellites, and then two different ways of fetching data are tried successively:

- From a local directory defined by the variable "HDFDIR". This way of fetching data is not used on the supercomputer and has been added for the desktop version of GFAS.
- If data was not found on the local directory, then it is fetched from the operational satellite data acquisition directory, maintained by the Operations Department (acq3:/acq3/scratch/acq3/lag/arch_ecfs/NASA). This is the common way of fetching data for NRT forecasts
- If the base time of the GFAS run is more than a few days before the current date, then data won't be available anymore on the operational satellite data acquisition directory. Then data is fetched from the ECFS, where a daily tar archive of raw satellite data is kept. This is how data is fetched for delayed mode forecasts on the supercomputer.

For MODIS data, the products fetched are:

- MOD14 : thermal Anomalies - fires and biomass burning, see documentation on the NASA website
- MOD03 : geolocation dataset, see documentation on the NASA website

Once the MODIS data has been fetched and de-tared if needed, symbolic links are created for each 5mn raw data file, so as to standardize file names for each satellite.

V. Gridding the data: firedo and associated scripts

Firedo is called for every 1-hour interval of the 24 hour assimilation window, which currently runs from 00:00 to 23:59 UTC of the base time, this one-hour interval is defined by theFIRE HH variable. As in fireget, a loop is done over the satellites (as defined by the "FRP_SAT" variable). For each 5mn raw MODIS data file comprised in the one-hour period, the following sequence is done:

- **MOD032geo** (compiled from Fortran 90 sources) extracts the geolocation information from the MOD03 raw data into an ascii file. This ascii file contains in the first line the number of valid observation points (2 values). The latitude, longitude and viewing angle are then entirely listed. This step is the most time-consuming of the GFAS system.
- If geolocation information from the MOD03 product is not available, then it is created from the MOD14 product by the **MOD142corners** shell script which uses the ncdump tool to extract the corner coordinates of the MODIS granule. If this step is successful then the latitude and longitude of all the pixels in the granule are computed by the **MODcorners2geo** executable (compiled from C sources) and stored into an ascii file with the same format as the one created by MOD032geo. For detected fires, the geolocation listed in MOD14 is reproduced. For the other pixels, the geolocation is approximated with an accuracy of about

15km. Since such geolocation data introduce a considerable error in the correction for partial cloud cover when processed at 0.1deg resolution, it is intended only as a back-up solution that increases the resilience of GFAS.

- The **MOD2list** executable (compiled from fortan90) then uses this geolocation ascii file together with the raw MOD14 data to produce a list of the pixels corresponding to the fire mask (ie where FRP values are positive or zero). The area corresponding to this pixel is also computed. An output file is produced which lists, for each pixel with a positive or vanishing FRP value :
    - latitude
    - longitude
    - FRP value
    - area of the pixel
    - viewing angle
- Finally, the list2grb executable (compiled from 2 different C sources: list2grb121120.c and idx_reg_ll100326.c) uses this list to grid the data to the 0.1° grid of the land-sea mask file. For each grid point, the active pixel is averaged using fraction of observed area as weights. Maximum FRP over the grid point is saved. The output is a 0.1° grib file that contains, for each grid point:
    - FRP
    - observation area
    - maximum FRP in the grid cell
    - mean viewing angle

The working directory for all these operations are the tmpFIREHH sub-directory of the working directory of the experiment, where FIREHH is the one-hour interval defined above. The final output of fireput, ie the 5mn gridded MODIS data for Terra and Aqua is copied into the grib sub-directory of the working directory of the experiment.

SEVIRI and Goes data can also be gridded by the firedo script. As these are not currently used in the pre-operational setup, the executable used for this gridding is not described here.

VI. Averaging: fireput and associated scripts

The fireput script loops over satellites as defined by the “FRP_SAT” variable, and also on the 24 one-hour periods of the assimilation window. It then calls the **average_grb_wei** executable (compiled from C) with the following arguments:

- the no-observation grib file
- the twelve 5mn FRP grib files of the one-hour period.

The **average_grb_wei** uses the first argument as a template: it provides the size of the output grib file. It then averages the first and the other arguments, using fraction of observed area as weights and saving the maximal FRP value. Thus the no-observation grib file is reproduced whenever no observations (and thus no 5mn grib files) are available. The hourly grib files for Terra and Aqua are created directly in the working directory of the experiment.

Once the loop over the hours is finished, **average_grb_wei** is called once more to average all the hourly data and produce a daily grib file for Terra and Aqua.

The hourly data is copied into grib files that contain only FRP and fraction of observed area, as only these parameters (and not the maximal FRP and viewing angle) are later used by Fire2emi.

VII. Assimilating FRP and computing the emissions of various species: fire2emi and scripts

Symbolic links are first created in the working directory, pointing towards the following files in the dat directory:

- the land-fraction file
- the gas flares data file
- the land cover type file
- the FRP analysis from the previous assimilation cycle (or the no-observation file if there are no data from the previous cycle)

The assimilation itself and the computation of the emissions are carried out by the python script **FRPassim2emi.py**, which relies heavily on functions of the **firegrib.py** script (both are in the bin directory). The python scripts are using the symbolic links mentioned above together with the hourly FRP and fire are data from Terra and Aqua that were produced by fireput. Quality control of the observations is at the time being de-activated in **FRPassim2emi.py**. The assimilation itself consists of the following sequence of actions:

- The hourly FRP observations from Terra and Aqua are merged (ie the fraction of observed area are added and the FRP observations are averaged, weighted by the fraction of observed area). This is carried out for all the observations, for daytime (9 to 21) and night time (21 to 9) observations.
- Gas flares are removed from the merged observations
- Observations of fires over water are removed and coastal grid cells are corrected
- A “forecast by persistence” is applied to the previous assimilation cycle’s FRP and fraction of observed area analysis. Fraction of observed area is divided by 10 during this forecast. This provides the background or first guess
- Today’s merged observations are merged with background from the previous step to produce a FRP and fraction of observed area analysis. As the fraction of observed area of the

"background" is much smaller, their relative weight in the merging operation is also much smaller as compared to the observations.

- The FRP analysis is converted into dry matter combustion rate using the land cover type information and conversion factors for each land cover coming from Heil et al., 2010.
- Dry matter combustion rate is converted into emission rates for 41 species using emission factors based on Andreae and Merlet (2001 and updates).

The FRP and fraction of observed area analysis is then copied to the dat directory.

VIII. Interpolating and archiving: fireputemi

Fireputemi archives into MARS the 0.1 ° hourly data for Terra and Aqua and also the 0.1° daily emissions for the 41 species. The daily FRP analysis and the merged observations for daytime and night time FRP are also archived.

0.5° fields are then interpolated from 0.1° using the remapping weight templates that were computed by firemake.

The same data as 0.1° is then archived at a 0.5° resolution.

IX. Description of the GFAS output archived in MARS

a) General aspects

The time of the data corresponds to the middle of the period covered by it, for example:

- Hourly data for 12utc consists of average data for the 12:00UTC to 12:55UTC will appear in MARS with timestamp 12:30
- Daily data will appear with timestamp 12UTC
- Data for the day-time will appear with time stamp 15UTC
- Data for the night-time will have a time stamps of 3UTC

The timestamp of the data is also different depending on the satellite:

- The minute is 1 for the first satellite (Aqua)
- It is 2 for the second satellite (Terra)
- It is 0 for merged data or analysis at a 0.1° resolution
- It is 9 for merged data or analysis at a 0.5° resolution

So, for example, hourly data for the 9:00 to 9:55 UTC period for the Terra satellite will have a 9:32 timestamp in MARS.

b) Description of the data

For Terra and Aqua, the following hourly observations are available in MARS:

- Mean FRP
- Fraction of observed area
- Maximum FRP
- Mean viewing angle

The following data is archived with both 0.1 and 0.5° resolution:

- Daily analysis of FRP, fraction of observed area and emissions of 41 species
- Merged observations for daytime and night time

X. KML files production: fireplot

The daily analysis of FRP is fetched from MARS, and KML is created by the **kmlFromGFAS.py** script.